

ARTICLE

# Modulation of tissue resident memory T cells by glucocorticoids after acute cellular rejection in lung transplantation

Mark E. Snyder<sup>1,2,5</sup> , Kaveh Moghbeli<sup>1</sup> , Anna Bondonese<sup>1</sup> , Andrew Craig<sup>1</sup> , Iulia Popescu<sup>1</sup> , Li Fan<sup>1</sup> , Tracy Tabib<sup>1</sup> , Robert Lafyatis<sup>1</sup> , Kong Chen<sup>1</sup> , Humberto E. Trejo Bittar<sup>3</sup> , Elizabeth Lendermon<sup>1</sup> , Joseph Pilewski<sup>1</sup> , Bruce Johnson<sup>1</sup> , Silpa Kilaru<sup>1</sup> , Yingze Zhang<sup>1</sup> , Pablo G. Sanchez<sup>4</sup> , Jonathan K. Alder<sup>1</sup> , Peter A. Sims<sup>6</sup> , and John F. McDyer<sup>1,5</sup> 

**Acute cellular rejection is common after lung transplantation and is associated with an increased risk of early chronic rejection. We present combined single-cell RNA and TCR sequencing on recipient-derived T cells obtained from the bronchoalveolar lavage of three lung transplant recipients with rejection and compare them with T cells obtained from the same patients after treatment of rejection with high-dose systemic glucocorticoids. At the time of rejection, we found an oligoclonal expansion of cytotoxic CD8<sup>+</sup> T cells that all persisted as tissue resident memory T cells after successful treatment. Persisting CD8<sup>+</sup> allograft-resident T cells have reduced gene expression for cytotoxic mediators after therapy with glucocorticoids but accumulate around airways. This clonal expansion is discordant with circulating T cell clonal expansion at the time of rejection, suggesting in situ expansion. We thus highlight the accumulation of cytotoxic, recipient-derived tissue resident memory T cells within the lung allograft that persist despite the administration of high-dose systemic glucocorticoids. The long-term clinical consequences of this persistence have yet to be characterized.**

## Introduction

Acute cellular rejection (ACR) is common after lung transplantation, occurring in 29% to 55% of recipients within the first year of transplantation (Martinu et al., 2009; Yusen et al., 2015). In addition to contributing to patient morbidity, ACR is associated with an increased risk of early chronic lung allograft dysfunction (CLAD), a progressive fibrosis of the small airways and the major limiting factor to long-term survival following lung transplantation. ACR is defined in lung transplant recipients as grades of perivascular or peribronchial infiltrates, predominantly composed of lymphocytes, found at the time of transbronchial biopsy. T cells are the predominant mediator of ACR in solid organ transplantation, including the lung (Marino et al., 2016; Weigt et al., 2019). Alloreactive T cells can be formed after priming by donor peptides presented by donor antigen-presenting cells (referred to as the direct pathway), donor peptides presented by recipient antigen-presenting cells (indirect pathway), or donor peptides presented on donor major histocompatibility complexes taken up by recipient antigen-presenting cells (semidirect pathway; Wakim and Bevan, 2011;

Alegre et al., 2016; Hughes et al., 2020; Snyder et al., 2022). The first-line treatment for ACR consists of high doses of glucocorticoids and/or augmentation of maintenance immunosuppression (Levine and Transplant/Immunology Network of the American College of Chest Physicians, 2004). In cases of advanced-grade ACR or ACR refractory to high-dose systemic glucocorticoids, lymphodepletive therapies such as anti-thymocyte globulin or monoclonal antibody to CD52 (alemtuzumab) can be effective treatment options (Reams et al., 2007).

Immediately after transplantation, circulating, recipient-derived T cells begin to populate the lung allograft, while the proportion of donor-derived tissue resident memory T cells (T<sub>RM</sub> cells) persisting in the lung allograft diminishes (Snyder et al., 2019). T<sub>RM</sub> cells are memory T cells that persist in either lymphoid or mucosal organs, do not recirculate, and are poised to have a rapid effector response in the setting of secondary challenge to pathogen (Schenkel and Masopust, 2014; Thome et al., 2014). Many of these lung-infiltrating recipient T cells upregulate canonical surface markers of T<sub>RM</sub> cells over the

<sup>1</sup>Department of Medicine, University of Pittsburgh, Pittsburgh, PA; <sup>2</sup>Department of Immunology, University of Pittsburgh, Pittsburgh, PA; <sup>3</sup>Department of Pathology, University of Pittsburgh, Pittsburgh, PA; <sup>4</sup>Department of Surgery, University of Pittsburgh, Pittsburgh, PA; <sup>5</sup>Starzl Transplantation Institute, University of Pittsburgh, Pittsburgh, PA; <sup>6</sup>Department of Systems Biology, Columbia University Irving Medical Center, New York, NY.

Correspondence to Mark E. Snyder: [snyderme2@upmc.edu](mailto:snyderme2@upmc.edu).

© 2022 Snyder et al. This article is distributed under the terms of an Attribution–Noncommercial–Share Alike–No Mirror Sites license for the first six months after the publication date (see <http://www.rupress.org/terms/>). After six months it is available under a Creative Commons License (Attribution–Noncommercial–Share Alike 4.0 International license, as described at <https://creativecommons.org/licenses/by-nc-sa/4.0/>).

months after transplantation and have gene expression similar to persisting donor-derived lung  $T_{RM}$  cells (Snyder et al., 2019). Importantly, the proportion of recipient-derived T cells in the lung allograft appears to correlate with the existence of ACR events; however, the specificity of recipient-derived T cells in the allograft has not been reported.

Using single-cell RNA and TCR sequencing of recipient-derived T cells found in the bronchoalveolar lavage (BAL) of patients with ACR and after successful treatment with methylprednisolone, we set out to determine whether recipient-derived T cells recruited to the lung allograft during ACR persisted as  $T_{RM}$  cells. Furthermore, we sought to compare gene expression of persisting recipient T cell clones before and after treatment with glucocorticoids. We found that at the time of ACR, the lung allograft contains a clonally expanded population of cytotoxic and effector  $CD8^+$  T cells that universally persist after successful treatment with glucocorticoids. These expanded clones are composed predominantly of effector memory T cells ( $T_{EM}$  cells), with rapid upregulation of gene and protein expression of canonical markers of tissue residency. Finally, we show that these clones are found to aggregate around the airways, consistent with lymphocytic bronchitis.

## Results

### Phenotype and localization of recipient-derived T cells during ACR

We first set out to determine the location and phenotype of recipient-derived T cells found in the allograft at the time of ACR and compare them with those found before ACR and after successful treatment with high-dose glucocorticoids. To accomplish this, we identified a cohort of 22 double lung transplant recipients for whom we had cryopreserved cells obtained from the BAL at the time of ACR and at least one sample from either before ACR or after successful treatment (Table 1). Most study participants had formalin-fixed, paraffin-embedded (FFPE) transbronchial biopsy specimens stored from the same time as BAL acquisition. We performed immunofluorescence imaging of CD3 and recipient HLA on FFPE transbronchial biopsies as well as multiparameter spectral flow cytometry characterization of recipient-derived T cells found in the BAL before, during, and after successful treatment for ACR. In both biopsies and BAL, recipient-derived T cells were isolated by staining for recipient-specific HLA (Fig. S1). From transbronchial biopsies clinically determined to have ACR, we found that perivascular lymphocytic infiltrates consisted mainly of recipient-derived  $CD3^+$  lymphocytes, with some donor-derived  $CD3^+$  lymphocytes seen within the parenchyma, more removed from the vascular space (Fig. 1 A). From the BAL, we found a statistically significant increase in the proportion of recipient-derived  $CD4^+$  T cells and a trend toward an increase in recipient-derived  $CD8^+$  T cells that did not reach statistical significance (Fig. 1 B).

We next performed recipient T cell phenotyping of serial BAL samples obtained from study participants who developed ACR. Based on cell surface CD45RA and CCR7 expression, T cells were divided into naive cells ( $CCR7^+CD45RA^+$ ),  $T_{EM}$  cells ( $CCR7^-CD45RA^-$ ), terminally differentiated effector T cells ( $CCR7^-CD45RA^+$ ), and

central memory T cells ( $T_{CM}$  cells;  $CCR7^+CD45RA^-$ ; Fig. 1 C). We found that the proportion of  $CD8^+$   $T_{EM}$  cells increased over the time course of ACR (Fig. 1, D and E) and that the majority of  $CD4^+$  T cells were composed of  $T_{EM}$  cells regardless of clinical state (Fig. 1, F and G). The two most reported canonical cell surface markers for  $T_{RM}$  cells in humans are CD69 (Kumar et al., 2017) and integrin  $\alpha E$  (CD103; Oja et al., 2018), with CD103 expression highlighting a subset of T cells that have a particularly rapid and robust effector response to secondary challenge with inhaled pathogens (Oja et al., 2018). We found no change in the BAL content of  $CD8^+$   $T_{RM}$  cells over the course of ACR (Fig. 1, H–J). Among  $CD4^+$  T cells, we found a decline in  $CD103^-CD4^+$   $T_{RM}$  cells after successful treatment of ACR, which occurred in parallel with a non-statistically significant increase in the proportion of  $CD103^+CD4^+$   $T_{RM}$  cells (Fig. 1, K and L).

### Clonally expanded T cells found in the BAL at the time of ACR invariably persist as $T_{RM}$ cells

To determine whether there is T cell clonal expansion within the lung allograft at the time of ACR, and if these expanded clones persist as  $T_{RM}$  cells, we performed single-cell RNA and TCR sequencing of FACS-sorted recipient-derived T cells found in the BAL of three study participants at the time of ACR and after successful treatment with systemic high-dose glucocorticoids (as well as one early sample predating ACR; Fig. 2 A). Any T cell clone persisting within the allograft across two time points was determined to be a definitive  $T_{RM}$  cell. We identified samples from two study participants with late (>1 yr) ACR and one from intermediate (6–12 mo) ACR. Late ACR samples were obtained 17 and 26 mo after transplantation, and intermediate ACR was obtained 10 mo after transplantation; follow-up BAL with associated biopsy showing clearance of ACR was obtained 2, 6, and 2 mo after ACR. Expanded clones were defined as any TCR clone (either TCR A/B pair or orphaned TCR  $\beta$ ) that consisted of >1% of the total recipient TCR repertoire at the time of BAL. We found oligoclonal T cell expansion in all seven samples, regardless of time frame and presence of ACR (Fig. 2, B–D; and Fig. S2 A). In study participant 8 (P8), for which we had an earlier sample, we found that the majority of expanded clones at the time of ACR were not present at earlier time points (Fig. 2 B). Importantly, in all three study participants, each expanded clone at the time of ACR persisted as a  $T_{RM}$  cell after successful treatment with high-dose systemic glucocorticoids (Fig. 2, B–D).

Using the TCR  $\beta$  sequence of the  $\alpha/\beta$  TCR pairs identified from our single-cell TCR analysis, we queried publicly available databases of HLA-conserved known viral-specific TCR  $\beta$  sequences (VDJdb, TBAdb, and McPAS-TCR; Shugay et al., 2018; Tickotsky et al., 2017). We further compared our identified sequences with groups of likely viral-specific CDR3 motifs using grouping of lymphocyte interactions by paratope hotspots (GLIPH; Glanville et al., 2017). We found that one study participant (P8) had an expansion of CMV-specific TCR clones early after transplantation, but none of the three participants had TCR expansion of either CMV- or EBV-specific T cells at the time of ACR (Fig. 2 E and Table S1). Flow cytometry analysis of five study participants comparing pre-ACR and ACR samples confirmed that there was no expansion of CMV- or EBV-specific

Table 1. Study participant demographics

ID	Age	Gender	Diagnosis	Induction	CMV (D/R)	Experiments
P1	40	F	Cystic Fibrosis	Alemtuzumab	-/-	SC, FC, BS
P2	50	F	Systemic Sclerosis	Basiliximab	+/+	FC
P3	21	F	Primary OB	Basiliximab	+/-	SC
P4	62	M	Primary OB	Basiliximab	+/-	FC
P5	65	F	IPF	Alemtuzumab	+/-	FC
P6	64	M	IPF	Alemtuzumab	+/+	FC
P7	66	F	Emphysema	Basiliximab	+/+	FC
P8	52	M	Systemic Sclerosis	Basiliximab	+/-	SC, IF, Bulk, FC, BS
P9	70	F	Emphysema	Alemtuzumab	+/+	IF
P10	69	M	IPF	Alemtuzumab	+/+	FC
P11	67	M	Emphysema	Alemtuzumab	-/-	FC
P12	31	M	Cystic Fibrosis	Basiliximab	+/-	IF
P13	54	M	Silicosis	Alemtuzumab	-/+	FC
P14	30	M	GVHD	Basiliximab	-/+	FC
P15	56	M	Sarcoidosis	Alemtuzumab	-/-	FC
P16	56	F	Emphysema	Basiliximab	+/-	IF
P17	30	F	Cystic Fibrosis	Alemtuzumab	+/+	IF
P18	62	M	IPF	Alemtuzumab	+/+	FC
P19	51	F	Other ILD	Basiliximab	+/-	FC
P20	68	M	IPF	Basiliximab	-/-	FC
P21	45	F	Emphysema	Alemtuzumab	-/-	FC
P22	62	M	Environmental	Basiliximab	+/-	FC

BS, BaseScope; Bulk, bulk TCR sequencing from PBMC; FC, flow cytometry; GVHD, graft versus host disease; IF, immunofluorescence imaging; IPF, idiopathic pulmonary fibrosis; OB, obstructive bronchiolitis; SC, single-cell RNA/TCR sequencing.

T cells at the time of ACR (Fig. 2 F). Future studies are required to definitively identify peptide specificity of these expanded clones found at the time of ACR, but they do not appear to be enriched for common herpesviruses.

#### Clonal expansion of cytotoxic CD8<sup>+</sup> T<sub>RM</sub> cells in the BAL during ACR

We next sought to determine the transcriptional phenotype of expanded clones at the time of late (>2 yr after transplantation) ACR using combined single-cell RNA and TCR sequencing of recipient-derived T cells obtained at the time of ACR and after successful treatment. From the BAL of P1 (obtained 26 mo after transplantation at ACR and 28 mo at time of treatment), we identified 10 distinct clusters of recipient-derived T cells based on single-cell transcriptional profiling (Fig. 3 A). Two distinct populations of clusters were identified, with the smaller population containing cells with an effector-memory gene expression profile and a larger population of clusters with gene expression more consistent with naive cells (based on *SIPRI* and *SELL* expression). The majority of T cell clonal expansion at the time of ACR was limited to the two most populous clusters within the Uniform Manifold Approximation and Projection (UMAP; Fig. 3 B, left). After successful treatment of ACR with high-dose systemic

glucocorticoids, clonal expansion persisted in, but was not limited to, the original two highly expanded clusters (Fig. 3 B, right). When highlighting the top four expanded clones within the UMAP, we found shared expansion of clones between clusters 0 and 1, all of which remained within the same cluster after treatment (Figs. 3 C and S2 B). When highlighting the top four clones expanded at the time of treatment, we found two clones persisting within clusters 0 and 1, as well as expansion of clones shared between clusters 3 and 4 (Figs. 3 D and S2 B). Overall, most expanded clones stayed within the same gene expression cluster, regardless of the presence or absence of ACR.

The two clusters containing the highest degree of T cell clonal expansion at the time of ACR had increased expression of *CD8A* (Fig. 3 E). Additionally, they had high expression of genes associated with cytotoxicity (*GZMB*, *GZMK*, and *PRFI*) and effector function (*IFNG*). Interestingly, these expanded clones had high increased expression of genes related to tissue residency (*ITGAE*, *ITGAI*, *PRDMI*, *CXCR6*, and *LAG3*) and downregulation of genes associated with tissue egress (*CCR7* and *SIPRI*), suggesting an early transcriptional signature favoring tissue retention. Interestingly, we found upregulation of *KLRC1*, the natural killer cell inhibitory receptor, which, in the context of viral infections, works to diminish viral-specific cytotoxicity (Moser et al., 2002).

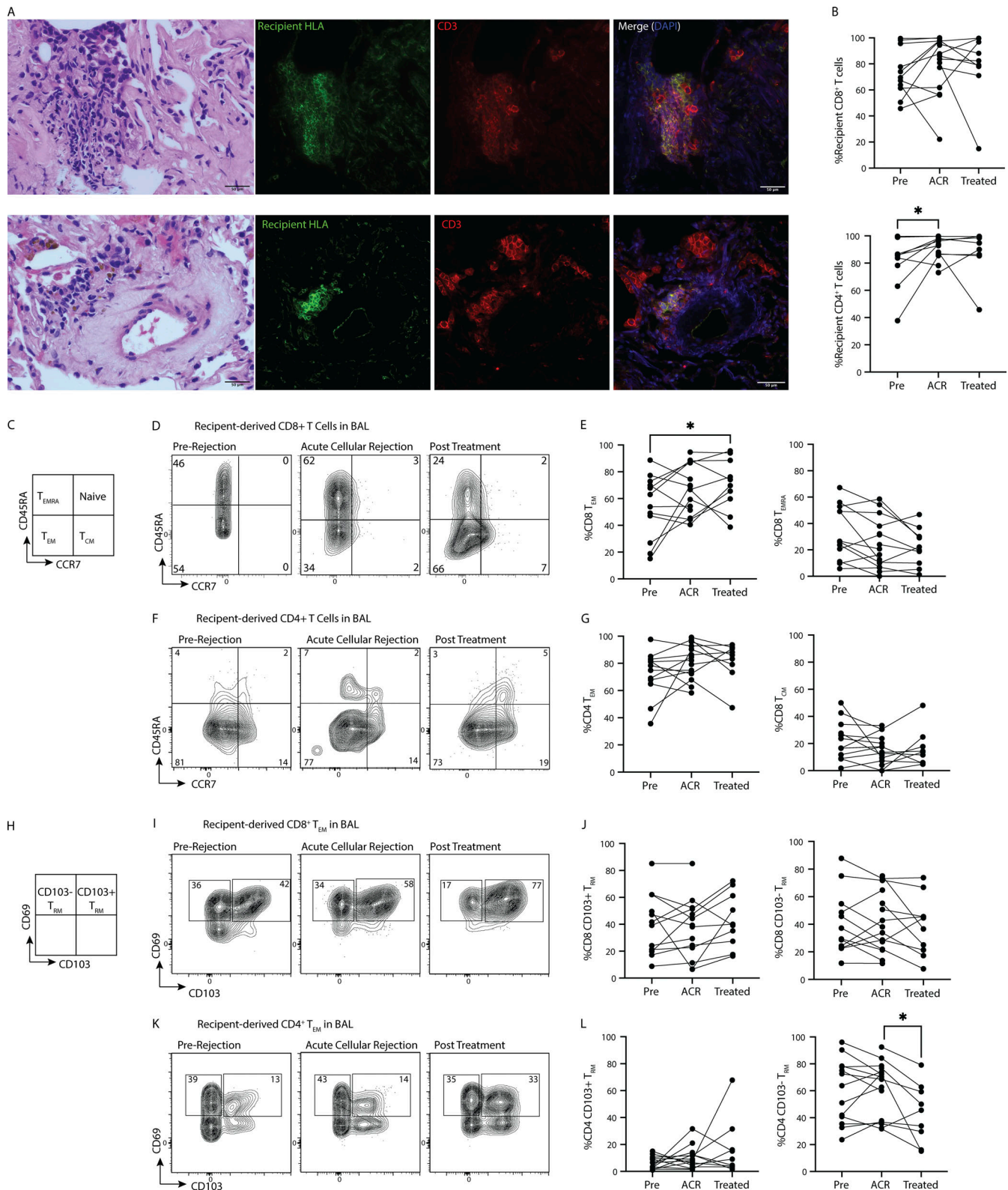


Figure 1. **Allograft infiltration by recipient-derived T<sub>EM</sub> cells during ACR.** (A) Immunofluorescence imaging of transbronchial biopsies from one study participant (P16) with ACR (top) and after treatment (bottom); green represents recipient-derived HLA (HLA-B7), and red represents CD3. Perivascular clusters of recipient-derived T cells (yellow cells on merged image) are seen in both images, but to a lesser extent after treatment. (B–L) Flow cytometry analysis of BAL comparing T cell phenotypes before, during, and after treatment for ACR. Comparisons include data from 17 study participants (n = 10 for before [pre] vs. ACR; n = 9 for ACR vs. treated; paired t test, \*, P < 0.05; no statistically significant difference if not indicated). (B) Proportion of recipient CD8<sup>+</sup> (top) and CD4<sup>+</sup> (bottom) T cells before, during, and after treatment for ACR. (C) Definition of T cell phenotypes based on CD45RA and CCR7 expression. (D) Representative flow cytometry of CD8<sup>+</sup> T cell phenotype from BAL before (left), during (center), and after (right) ACR. (E) Cumulative data of CD8<sup>+</sup> T cell phenotype (T<sub>EM</sub> left;

$T_{CM}$  right). **(F)** Representative flow cytometry of  $CD4^+$  T cells from BAL before (left), during (center), and after (right) ACR. **(G)** Cumulative data of  $CD4^+$  T cell phenotypes ( $T_{EM}$  left;  $T_{CM}$  right). **(H)** Defining different phenotypes of  $T_{RM}$  cells based on CD69 and CD103 expression. **(I)** Representative flow cytometry of  $CD8^+$   $T_{RM}$  from the BAL before (left), during (center), and after (right) ACR. **(J)** Cumulative data of  $CD8^+$   $T_{RM}$  cells (CD103<sup>+</sup> left; CD103<sup>-</sup> right). **(K)** Representative flow cytometry of  $CD4^+$   $T_{RM}$  cells from the BAL before (left), during (center), and after (right) ACR. **(L)** Cumulative data of  $CD4^+$   $T_{RM}$  cells (CD103<sup>+</sup> left; CD103<sup>-</sup> right).

Clusters 3 and 4 displayed more clonal expansion at the time of successful treatment and had genes upregulated for *TNFRSF4*, suggesting  $CD4^+$  T cells, as well as *CCR7* and *SIPRI*, consistent with a naive phenotype (Fig. 3 E). When we performed subset analysis of the top four clones at the time of ACR and compared gene expression from these persisting clones between ACR and treatment, we found that these expanded clones downregulated genes related to cytotoxicity (*GZMB* and *PRFI*; Fig. 3 F). The most upregulated gene after treatment was *CRIP1*. Together, these findings show that during ACR, the allograft contains a clonal expansion of cytotoxic, recipient-derived  $CD8^+$  T cells, which all persist as  $T_{RM}$  cells after successful treatment of clinical ACR with high-dose systemic glucocorticoids, but with reduced expression of functional markers of cytotoxicity.

#### Differential clonal expansion in the allograft vs. the circulation

One prior study in kidney transplant recipients showed shared clonal expansion in the renal allograft and circulation during ACR (Alachkar et al., 2016). To determine whether this relationship was true in the lung allograft, we compared the TCR repertoire from the BAL of P2 with the bulk TCR  $\beta$  chain repertoire obtained from circulating recipient-derived T cells 3, 9, and 16 mo (the time of ACR) after transplantation. From the BAL, we found clonal expansion of cytotoxic  $CD8^+$   $T_{RM}$  cells, similar to findings in P1 (Fig. 4, A and B). Like P1, all expanded clones persisted, albeit at reduced frequencies, after successful treatment of ACR with high-dose methylprednisolone (Fig. 4 C).

Bulk TCR  $\beta$  sequencing was next performed from DNA isolated from FACS-sorted, circulating, recipient-derived T cells from this same transplant recipient at different time points, including at the time of ACR. This was performed both on all T cells and on  $CD69^+$  and/or  $CD137/CD40L^+$  T cells after a 12-h mixed lymphocyte reaction with irradiated donor cells.  $CD69^+$  and/or  $CD137^+$  cells were labeled allo-specific. We found a polyclonal population of expanded alloreactive T cells at the time of ACR (16 mo), most of which were not present 3 mo after transplant (Fig. 4 D), but most of which were already present 9 mo of transplant (Fig. 4 E). Most of the expanded circulating T cell clones at the time of ACR were alloreactive (Fig. 4 F). At the time of ACR, there was oligoclonal expansion of previously identified circulating T cell clones (Fig. 4 G). However, of the top expanded clones in the circulation, only a fraction were identified within the BAL and, when present, were not clonally expanded (Fig. 4 H). Of 328 shared TCR  $\beta$  sequences identified between the BAL and circulation at the time of ACR, only 10 had >10 copies in the BAL; all 10 of these clones were rare in the circulation (<0.1% frequency).

#### Expanded clones migrate to the airways

To determine the anatomic localization of expanded T cell clones, we used a BaseScope in situ hybridization assay

(Advanced Cell Diagnostics) with an RNA probe for the CDR3 $\beta$  region of the top expanded clone identified in the BAL of P1 and P8 at the time of ACR. We performed in situ hybridization using this probe on FFPE transbronchial biopsies obtained from P1 at four time points (8 and 19 mo after transplantation without ACR, 27 mo with ACR, and 28 mo after treatment). The specific T cell clone was seen at all time points measured, but with non-airway expansion at the time of ACR and airway enrichment after treatment (total count: airway at 8 mo without ACR, 3:1; 19 mo without ACR, 2:2; 27 mo with ACR, 13:0 [Fig. 5 A]; and 28 mo after treatment, 108:28 [Fig. 5 B]). P8 biopsies were analyzed at five timepoints (2 and 7 mo after transplantation without ACR, 17 mo with ACR, and 19 and 23 mo after treatment). The clone of interest was not visualized in the two samples obtained before developing ACR but was seen at the time of ACR and at both time points after treatment. Again, we saw more airway localization after treatment (total count: airway at 17 mo with ACR, 6:2; 19 mo, 11:5; and 23 mo, 13:9 [Fig. S3]). This suggests that expanded T cell clones found in the lung at the time of ACR migrate to the airways and persist as  $T_{RM}$  cells.

#### Transcriptional reprogramming of persisting clones after systemic glucocorticoid therapy for ACR

We next set out to identify the transcriptional signature of expanded clones in relation to nonexpanded clones at the time of ACR and in relation to the same clones after successful treatment of ACR in concatenated samples of all three study participants. First, we identified the top four expanded clones from all three study participants at the time of ACR (Fig. 6 A). Comparing gene expression in the expanded clones vs. all other T cells found in the BAL, we found that expanded clones had upregulation of genes associated with cytotoxicity (*GZMB*, *GZMH*, *PRFI*, and *NKG7*), leukocyte migration (*CCL5*, *XCL1*, and *XCL2*), cellular activation (*HLA-DRB1*), tissue residency (*ITGAE*), and cellular exhaustion (*LAG3*). Genes downregulated in expanded clones included those related to tissue egress (*CCR7*) and one associated with cytotoxicity (*KLRB1*; Fig. 6 B).

Next, we focused our analysis on the top four clones identified from each BAL sample at the time of ACR and compared gene expression from those 12 clones with the same clones identified after successful treatment with methylprednisolone (Fig. 6 C). Comparing the same clones before and after treatment, we found upregulation of genes at the time of ACR related to cytotoxicity (*GZMB*, *GZMK*, *PRFI*, and *LAMP1*), effector function (*IFNG* and *TNF*), and cellular exhaustion (*PDCD1* and *LAG3*) and transcription factors associated with effector function (*TBX21* and *EOMES*). The two most upregulated genes after successful treatment were *CRIP1* and *NME2* (Fig. 6 D). These findings support that allograft-persisting  $CD8^+$   $T_{RM}$  cells are transcriptionally reprogrammed after clinical clearance of ACR

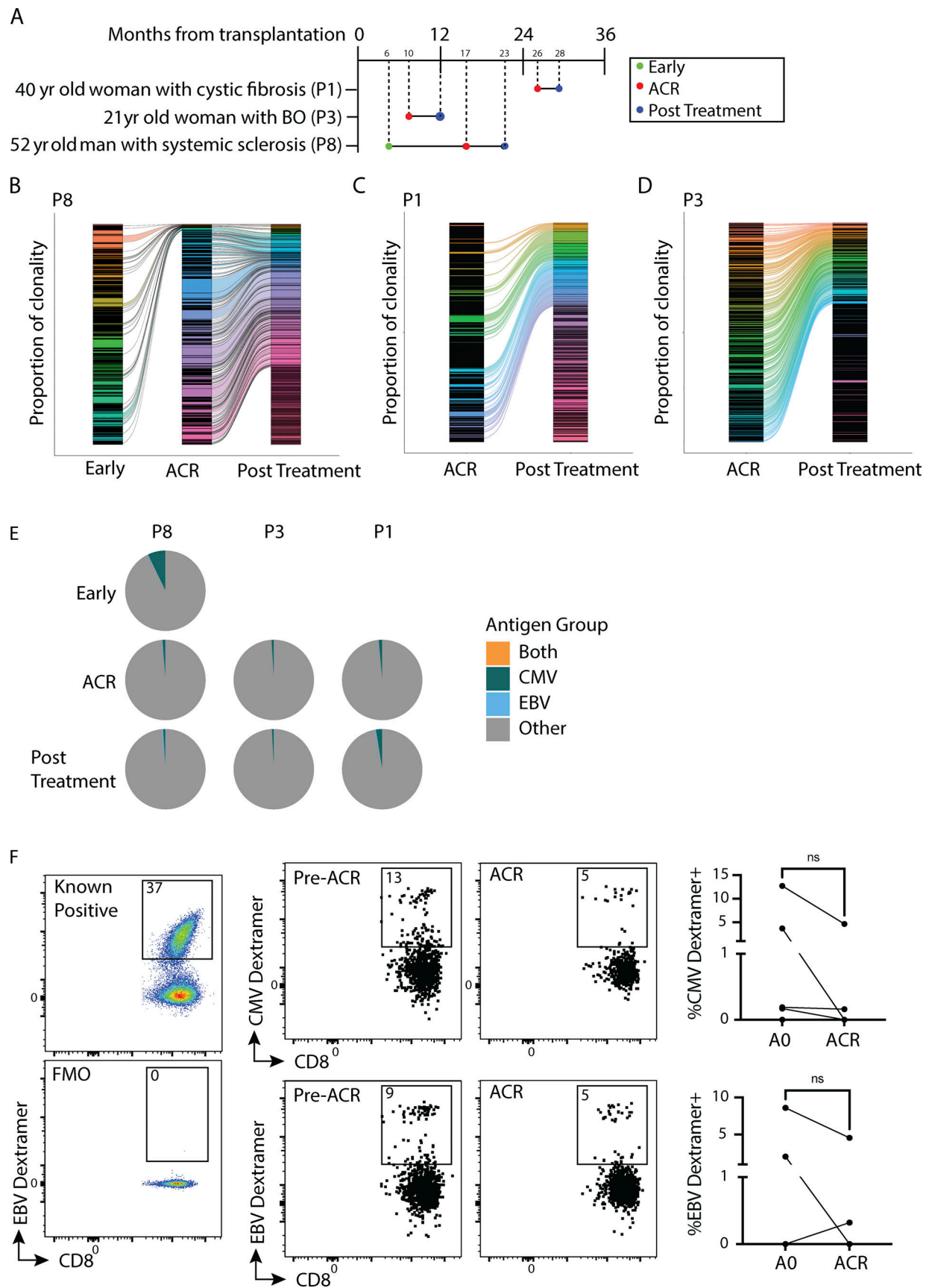


Figure 2. **Clonally expanded recipient-derived T cells at the time of ACR persist as  $T_{RM}$  cells.** (A) Experimental design outlining longitudinal sampling for single-cell RNA and TCR sequencing of recipient-derived T cells found in the BAL of lung transplant recipients. BO, bronchiolitis obliterans. (B–D) Recipient-

derived T cell clonal overlap from longitudinal BAL samples obtained from three study participants, P8 (B; left, with three time points 6, 17, and 23 mo after transplantation), P1 (C; center, with two time points 26 and 28 mo after transplantation), and P3 (D; right, with two time points 10 and 12 mo after transplantation). Each color represents a unique clonotype; TCR  $\alpha$ /TCR  $\beta$  pairs and orphaned TCR  $\beta$  are included separately in the analysis. **(E)** Distribution of CMV- and EBV-specific TCR by participant and study time frame, represented by frequencies of clones identified by querying public databases of HLA-conserved, viral-specific TCR  $\beta$  sequences (databases include VDJdb, TBADb, and McPAS-TCR). **(F)** Flow cytometry viral dextramer analysis of 10 BAL samples obtained from five study participants for CMV and four participants for EBV (comparing pre-ACR to ACR). CMV dextramer, HLA-A\*0201-NLVPMTATV (HLA-A\*0301-KLGGALQK)/PE conjugated; EBV dextramer, HLA-A\*0201 - GLCTLVAML (BMLF1 protein); FMO, fluorescence minus one (excluding viral dextramer); known positive, previously identified, known EBV PCR<sup>+</sup> transplant recipient not included in the cumulative analysis.

with high-dose systemic glucocorticoids. It remains unknown whether this is an effect, either direct or indirect, of glucocorticoid therapy or whether it is a conditioned response from local drivers or persistent antigen exposure.

### Production of cytotoxic mediators correlates with transcriptional profile

Transcriptional analysis of recipient T cells found in the BAL at the time of ACR clearly identify a clonally expanded population of CD8<sup>+</sup> T cells with a transcriptional profile suggesting a cytotoxic T<sub>RM</sub> cell phenotype. To determine if the protein production of recipient-derived T cells in the BAL during ACR correlates with gene expression, we performed multiparameter flow cytometry on unstimulated cells derived from five patients at the time of ACR and compared the results with BAL T cells obtained from the same five patients after successful treatment of ACR. A total of 36,521 live, recipient-derived CD3<sup>+</sup> T cells from 10 samples obtained from 5 study participants (range of 1,945–16,391 cells per participant) were included in a concatenated t-distributed neighbor embedding (tSNE) 2D reduction of protein expression. There was a near-equal proportion of CD8<sup>+</sup> and CD4<sup>+</sup> T cells found in the BAL, the majority of which were T<sub>EM</sub> cells, with one cluster of cells found predominantly during ACR (Fig. 7 A). All study participants had T cells within the ACR-enriched cluster, but to varying degrees, with three participants having a much greater proportion (Fig. S4, A and B). The cluster of cells relatively unique to ACR were found to have increased cell surface expression of CD69, but not CD103 (Fig. 7 B). These cells had low expression of Ki67, suggesting they were not proliferating. This same cluster of ACR-specific cells had a high quantity of mediators of cytotoxicity (granzyme B, granzyme K, and perforin) as well as increased surface expression of KLRC1, a protein believed to be instrumental in negative feedback of natural killer cells (Fig. 7 C). Immunofluorescence imaging of transbronchial biopsies obtained at the time of ACR show that pathognomonic lesions for ACR (perivascular infiltrate of lymphocytes) were predominantly composed of recipient-derived T cells with high expression for granzyme B (Fig. 8 A), with airway-centered T cells with similarly high content of granzyme B (Fig. S4 C).

Cysteine-rich intestinal protein 1 (CRIP1) is an incompletely characterized double zinc-finger LIM protein that is abundantly expressed in the intestines and peripheral blood mononuclear cells (PBMCs; Hallquist et al., 1996). We found that CRIP1 was the most consistently upregulated gene in persisting recipient-derived T<sub>RM</sub> cells within the BAL. When performing immunofluorescence imaging of transbronchial biopsy specimens, we found substantial but noncellular specific content of the CRIP1

protein (Fig. 8 B). After successful treatment of ACR with methylprednisolone, however, we saw increased colocalization of the CRIP1 protein with lung T cells (Fig. 8 C and Fig. S4, D and E). Together, these findings confirm that, during ACR, the lung contains a clonally expanded population of cytotoxic, recipient-derived CD8<sup>+</sup> T cells that universally persist in the lung as T<sub>RM</sub> cells after successful treatment with high-dose glucocorticoids. After treatment, the lung T cell population downregulates gene and protein expression of cytotoxic mediators and upregulates CRIP1.

### Discussion

ACR represents a major burden to patient morbidity after lung transplantation and is associated with an increased risk of early CLAD, the major limiting factor to long-term survival after transplantation. Herein, we show that ACR of lung allografts is notable for a perivascular infiltrate of recipient-derived CD3<sup>+</sup> lymphocytes, most of which have a T<sub>EM</sub> cell phenotype, followed by a terminally differentiated effector population. From single-cell RNA/TCR sequencing of recipient-derived T cells obtained in the BAL of three study participants with active ACR, we show that ACR is characterized by oligoclonal CD8<sup>+</sup> T cell expansion within the allograft, with expanded clones having a cytotoxic gene expression and protein production, dominated by granzyme B, granzyme K, and perforin. We found that, in all three study participants, all expanded clones (>1% of the total clonal population) persisted as T<sub>RM</sub> cells weeks to months after successful treatment with high-dose systemic glucocorticoids—however, with a reprogrammed transcriptional profile. The most highly expanded clones, identified from two separate study participants, were noted on biopsy to migrate to the airways after treatment. Finally, we show that clonal expansion within the allograft was discordant with oligoclonal expansion in the periphery at the time of ACR. Together, these findings suggest that cytotoxic T cells recruited to the allograft during ACR develop into lung T<sub>RM</sub> cells that persist despite high-dose systemic glucocorticoids.

We previously reported that over the months following lung transplantation, graft-infiltrating, recipient-derived T cells develop a phenotype of tissue residency, upregulating proteins that promote tissue retention (Snyder et al., 2019). These include CD69, which promotes downregulation of the protein SIPR1, thereby diminishing lymphatic egress (Skon et al., 2013); CD103 (integrin  $\alpha$  E), which binds to E cadherin, promoting retention near epithelial cells (Cepek et al., 1994; Strauch et al., 2001); and CD49 (integrin  $\alpha$  1), which promotes retention by binding to collagen (Gullberg et al., 1992; Reilly et al., 2020). Importantly,

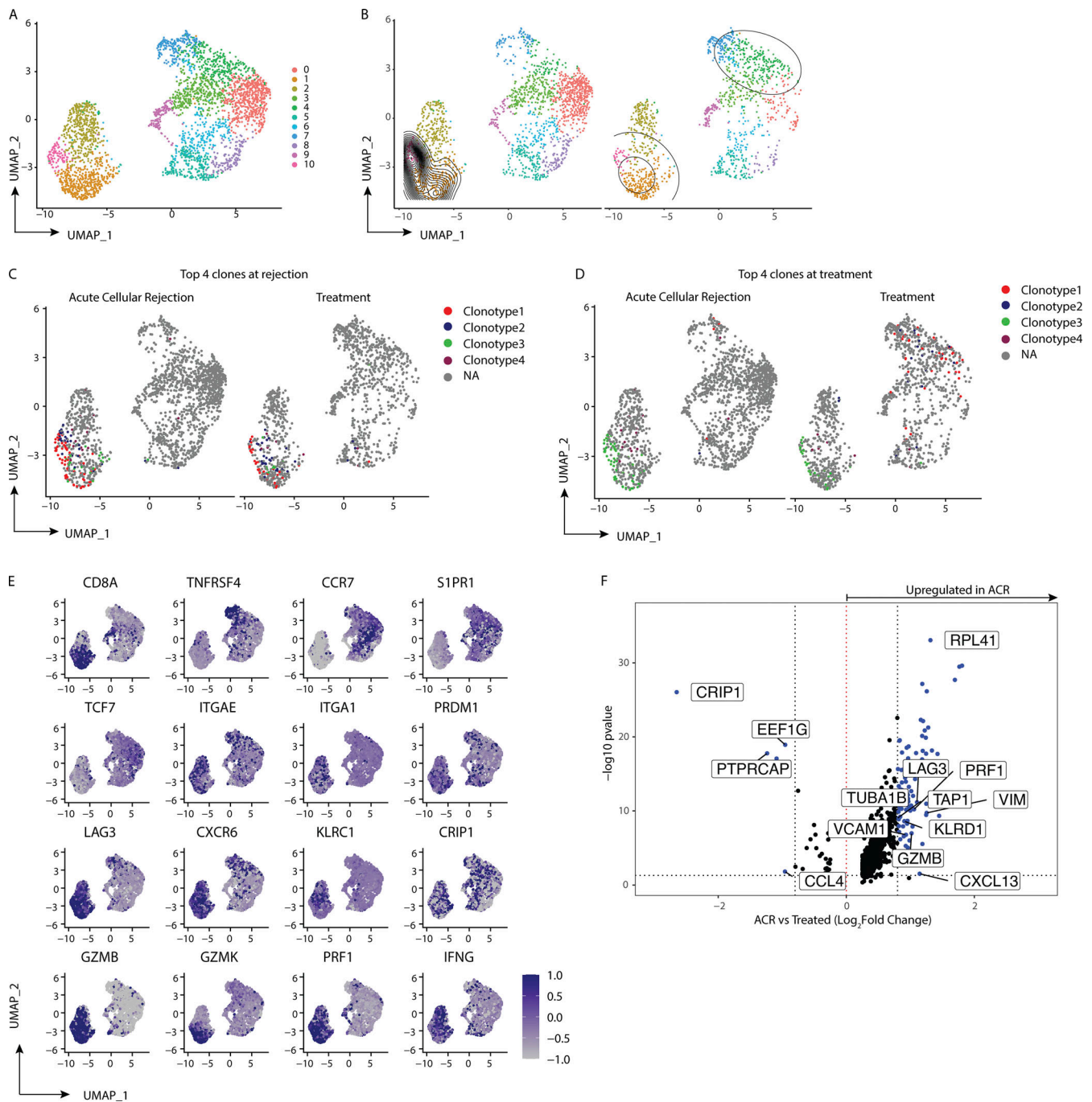


**Figure 3. Clonal expansion of cytotoxic CD8<sup>+</sup> T cells during ACR that persist as T<sub>RM</sub> cells.** (A) UMAP of concatenated samples from study participant P1 at the time of ACR and after treatment, showing 10 distinct clusters of recipient-derived T cells. (B) Density plot of clonal expansion overlaying UMAP, separated by cells obtained at the time of ACR (left) and after treatment (right). (C) UMAP separated by ACR (left) and treatment (right) samples highlighting the top four clonotypes present at the time of ACR (paired TCR  $\alpha$ /TCR  $\beta$  and orphaned TCR  $\beta$  are combined by shared TCR  $\beta$ ). (D) UMAP separated by ACR (left) and treatment (right) samples highlighting the top four clonotypes present at the time of treatment (paired TCR  $\alpha$ /TCR  $\beta$  and orphaned TCR  $\beta$  are combined by shared TCR  $\beta$ ). (E) Feature plots of concatenated samples from participant P1. (F) Volcano plot showing differential gene expression between ACR and treatment using subset of top four clones at the time of ACR.

this accumulation of recipient-derived T cells in the allograft occurred faster in the setting of ACR (Snyder et al., 2019). In a murine model of delayed rejection after orthotopic renal transplantation, polyclonal, antigen-specific CD8<sup>+</sup> T<sub>RM</sub> cells populated the graft and contributed to the development of chronic rejection (Abou-Daya et al., 2021). Furthermore, renal allografts after

human transplantation contained CD8<sup>+</sup> T<sub>RM</sub> cells that could produce large amounts of granzyme B, perforin, IFN $\gamma$ , and TNF $\alpha$  after stimulation with the phorbol ester, PMA/ionomycin (de Leur et al., 2019). Our finding that clonally expanded CD8<sup>+</sup> T cells found during ACR persist as T<sub>RM</sub> cells and migrate to the airways suggests a plausible biologic mechanism whereby ACR

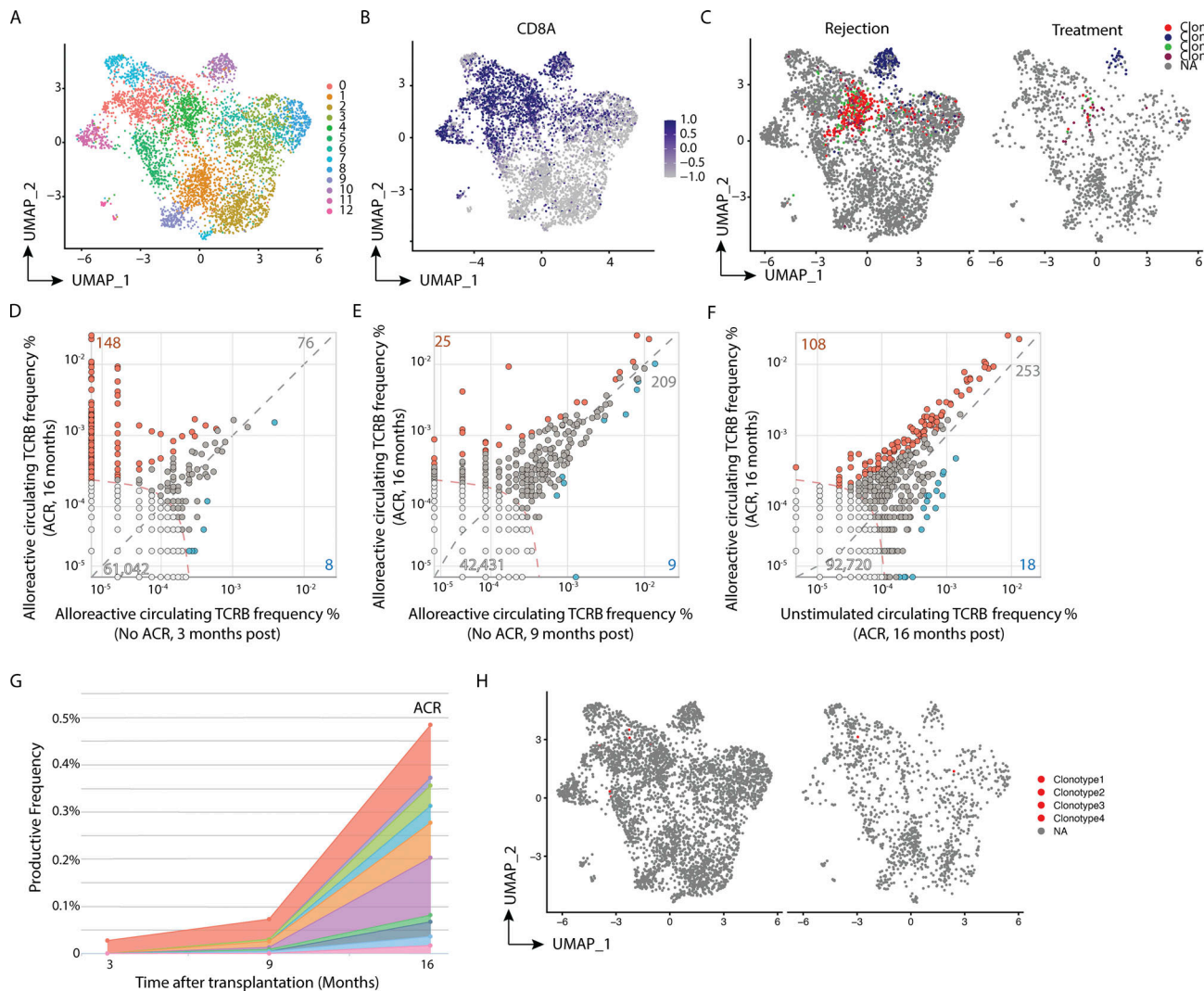


**Figure 4. T cell clonal expansion is discordant between allograft and circulation at ACR. (A)** UMAP of concatenated samples from study participant P8 at the time of ACR and after treatment, showing 12 distinct clusters of recipient-derived T cells. **(B)** Feature plot highlighting CD8<sup>+</sup> T cells. **(C)** UMAP separated by ACR (left) and treatment (right) samples, highlighting the top four clonotypes present at the time of treatment (paired TCR  $\alpha$ /TCR  $\beta$  (TCRB) and orphaned TCR  $\beta$  are combined by shared TCR  $\beta$ ). **(D–F)** Scatterplots of bulk TCR  $\beta$  sequencing from DNA extracted from FACS-sorted circulating T cells obtained from study participant P8 3, 9, and 16 mo (at time of ACR) after lung transplantation. For each scatterplot, orange data points represent alloreactive clones expanded at the time of ACR, blue data points represent clones less prevalent at the time of ACR, and gray data points represent clones expanded in both groups. Any datapoint on the x or y axis represents a unique clone to that sample. **(D)** Alloreactive clones at the time of ACR (y axis) compared with alloreactive clones found at 3 mo (x axis). **(E)** Alloreactive clones at the time of ACR (y axis) compared with alloreactive clones at 9 mo. **(F)** Alloreactive clones at time of ACR (y axis) compared with all clones found at time of ACR (x axis). **(G)** Clonal overlap of expanded alloreactive clones 3 to 16 mo after transplantation. **(H)** UMAP separated by ACR (left) and treatment (right) samples of T cells in BAL, highlighting the top expanded clonotypes present in the circulation at the time of ACR (paired TCR  $\alpha$ /TCR  $\beta$  and orphaned TCR  $\beta$  are combined by shared TCR  $\beta$ ).

contributes to the bronchiolitis obliterans syndrome phenotype of CLAD. Indeed, we recently demonstrated a strong type 1 immunity gene signature using bulk RNA sequencing (RNAseq) obtained from airway brushings of the distal small airways in patients with CLAD, consistent with these findings (Iasella et al., 2021). Although the T<sub>RM</sub> cells appear to undergo transcriptional reprogramming after systemic glucocorticoid therapy, further study is required to see whether, like other T<sub>RM</sub> cells, they are capable of rapid reactivation.

Bulk RNA sequencing of the cellular component of BAL from lung transplant recipients with and without ACR previously identified genes related to cellular cytotoxicity to be upregulated

during ACR, most notably *GZMK* and *GZMA*, as well as effector gene *IFNG* (Weigt et al., 2019). Despite this cytotoxic transcriptional profile, we cannot definitively say that the expanded clonal population found in the allograft at the time of ACR is composed entirely of alloreactive clones. The oligoclonal nature of the expansion, as well as the discordant clonal expansion from circulating T cells, would suggest that this does not represent bystander activation. This discordant clonal expansion, however, does raise the possibility of local expansion of previously established T<sub>RM</sub> cells as a possible source, which has been shown to occur in a murine model of recurrent skin infections (Park et al., 2018). Renal transplant studies have shown CMV-specific

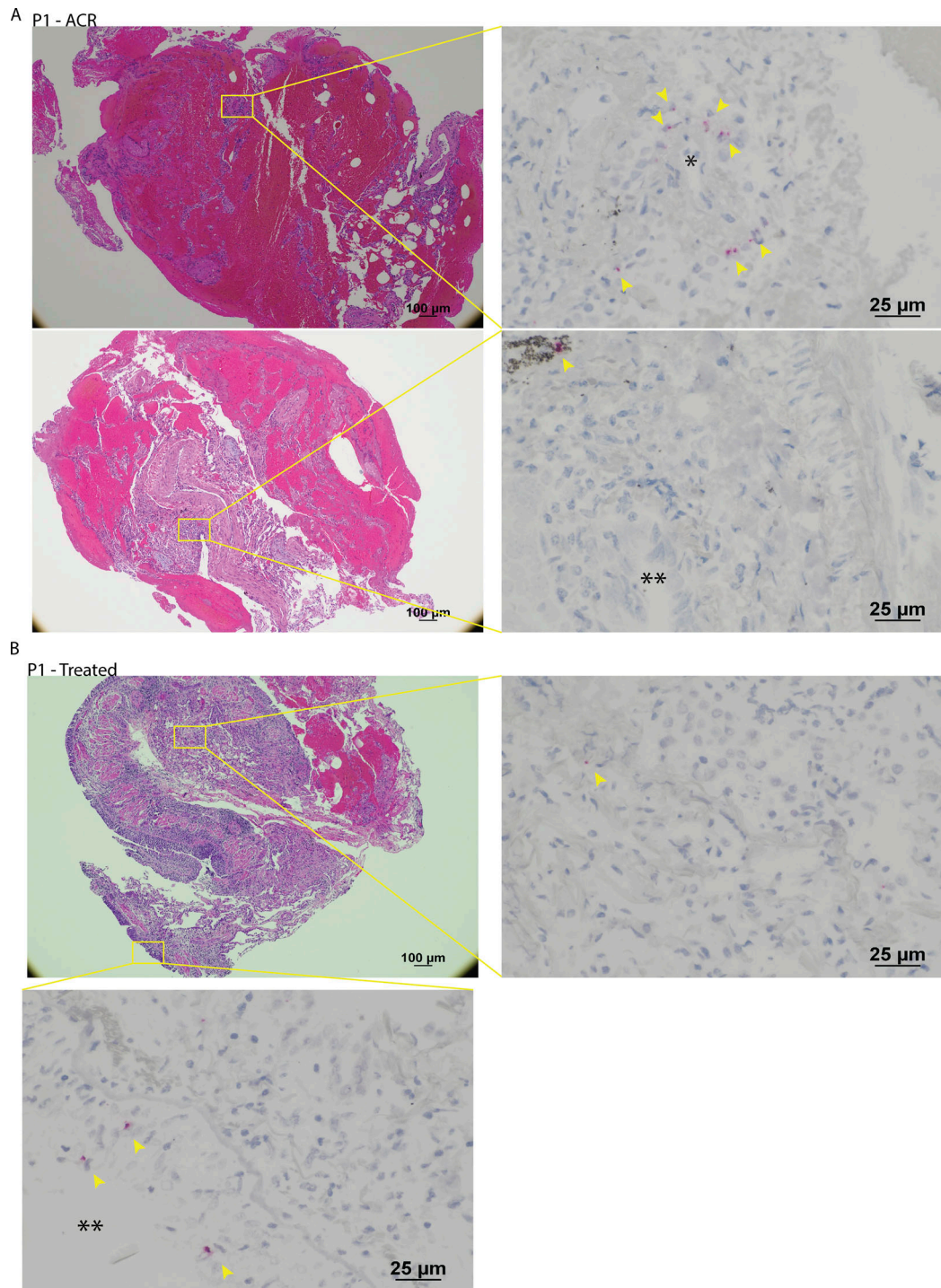


Figure 5. **Top expanded clonotype at ACR persists in the airway as  $T_{RM}$  cells.** (A) 4× H&E stain of transbronchial biopsy of study participant P1 at the time of ACR (top and bottom left) and 40× RNA in situ hybridization (right, BaseScope) highlighting a blood vessel (\*) surrounded by 10 copies of the specific TCR clone (top right) and two copies of the clone >50 mm from the airway (\*\*, bottom right). (B) 4× H&E stain of transbronchial biopsy of study participant P1 after successful treatment of ACR (top left) and 40× RNA in situ hybridization (bottom left and top right, BaseScope) highlighting an isolated copy of the clone within the lung parenchyma (top right) and three copies of the clone within the intra-epithelial layer of the airway (\*\*, bottom left). Yellow arrowheads point to positive staining (red dots).

T cells to have cross-reactivity with the allograft (Stranavova et al., 2019), or other inhaled viral pathogens or microbiome. Our results from both flow cytometry and TCR repertoire analysis, based on a limited cohort, would suggest that CMV- or EBV-specific T cells do

not greatly contribute to the allograft clonal expansion at the time of ACR. Due to the paucity of cryopreserved cells, we were unable to perform proliferation studies on these samples to definitively determine alloreactive potential.

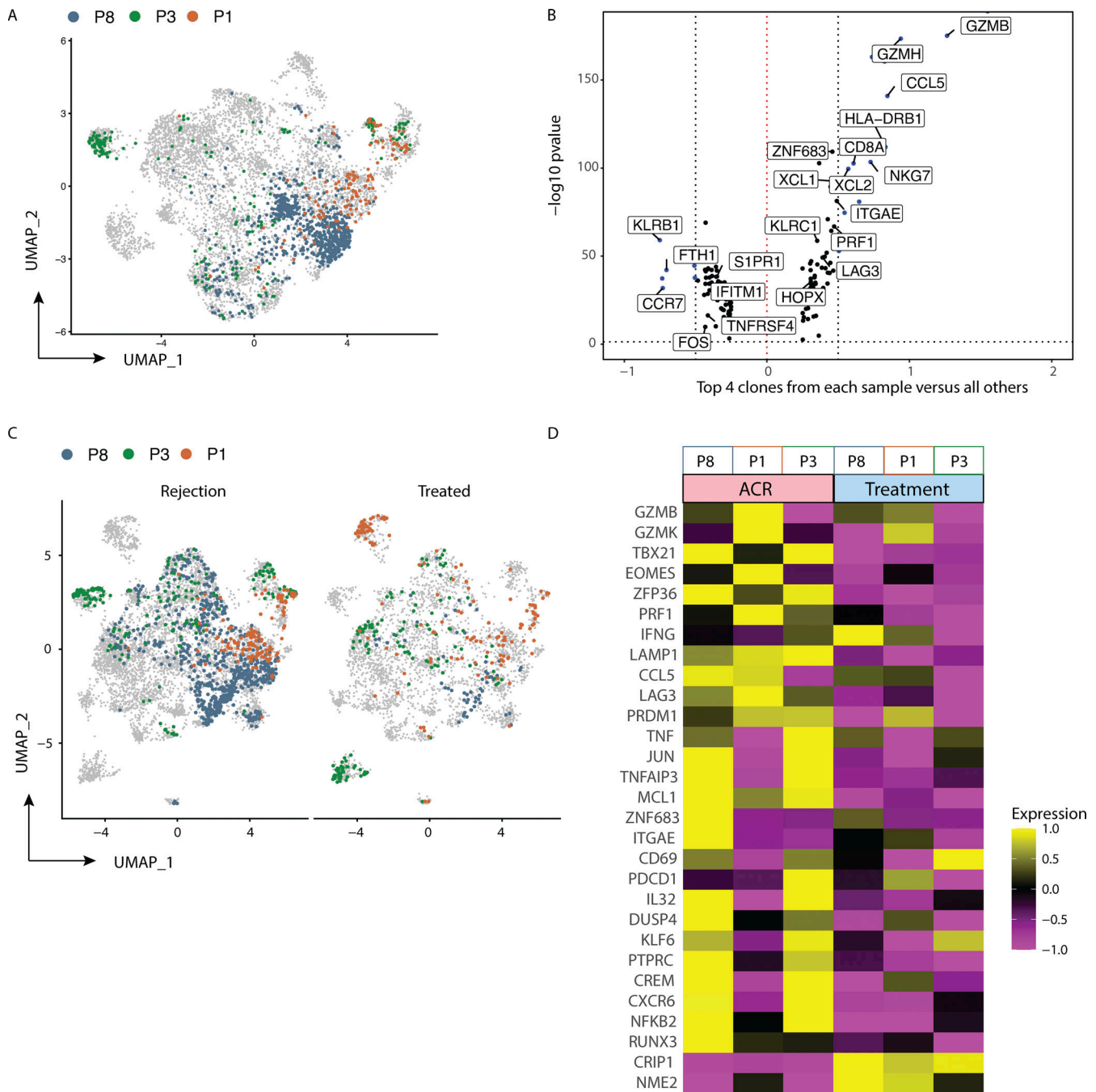


Figure 6. **Transcriptional reprogramming of lung  $T_{RM}$  cells after high-dose systemic glucocorticoids.** (A) UMAP of concatenated samples from three study participants, P8, P1, and P3, at the time of ACR. (B) Volcano plot showing differential gene expression between top four clones from each sample at the time of ACR compared with all other clonotypes found at the time of ACR. (C) UMAP of concatenated samples from both ACR and treatment samples from three study participants, P8, P1, and P3, split by presence of ACR (left) and samples obtained at time of successful treatment (right). (D) Heatmap over averaged gene expression comparing the top four clones at the time of ACR for all three samples compared with those same clones at the time of treatment.

The clinical management of ACR after lung transplantation varies greatly by institution and individual provider (Levine and Transplant/Immunology Network of the American College of Chest Physicians, 2004). Despite this heterogeneity in clinical approach, systemic glucocorticoids remain the standard first-line therapy for symptomatic ACR (Martinu et al., 2011). The use of glucocorticoids to treat ACR is largely based on extrapolation from kidney transplant practice and serial pathologic

assessments of lung allografts showing diminished perivascular infiltration after treatment (Clelland et al., 1990). The impact of systemic glucocorticoids on diminishing ACR has been postulated as an effect on circulating T cells, both diminishing the number of alloreactive cells via apoptosis (Migita et al., 1997) and reducing the activation and cytokine production of alloreactive cells via inhibition of IL2 signaling and production (Paliogianni et al., 1993).  $T_{RM}$  cells represent a unique subset of memory

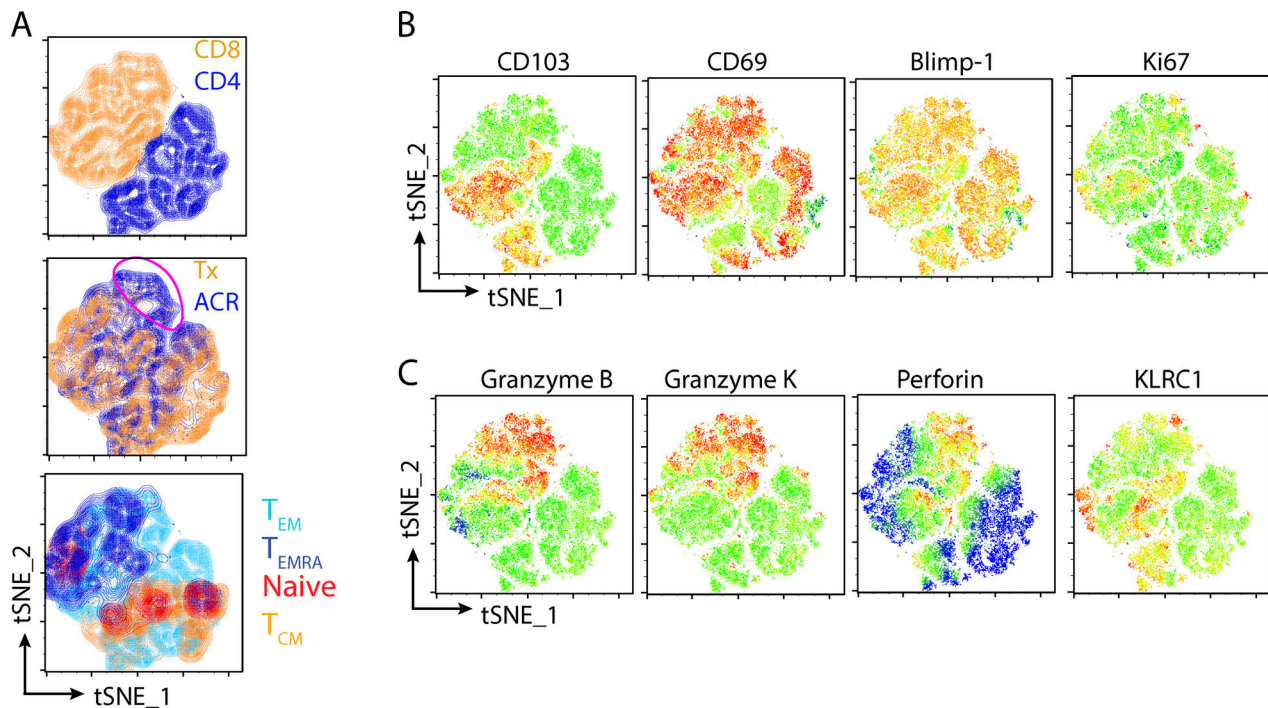


Figure 7. **Recipient T cells at ACR have high content of cytotoxic mediators.** (A–C) tSNE of 10 concatenated flow cytometry samples obtained from five study participants (each sample has one at the time of ACR and one after successful treatment), including 36,521 total cells. (A) tSNE showing T cell phenotype from 10 samples (encircled cluster in middle plot highlights ACR-enriched cluster of CD8<sup>+</sup> T<sub>EM</sub> cells). (B) tSNE highlighting proteins related to tissue residency (CD103, CD69, and Blimp-1), and proliferation (Ki67). (C) tSNE highlighting cytotoxic mediators (granzyme B, granzyme K, and perforin), and presumed self-regulatory protein KLRC1.

T cells that are relatively removed from the circulation, even in the highly vascular human lung (Snyder et al., 2021). This sparing from the circulation is believed to be the reason that T<sub>RM</sub> cells are relatively protected from the effects of some systemic lymphodepletive therapies (Clark et al., 2012). The effect of systemic glucocorticoids on mucosal T<sub>RM</sub> cells has yet to be reported. Here, we show a transcriptional reprogramming of lung T<sub>RM</sub> cells after the administration of high-dose glucocorticoids, suggesting an impact on local resident immunity. It remains unclear whether this is a direct effect of glucocorticoids on the T<sub>RM</sub> cells or an indirect effect via circulating impaired helper T cells (Mahata et al., 2014) or regulatory T cells (Bereshchenko et al., 2014) or through impacts on the local environment. Further study is required to elucidate how systemic glucocorticoids impact mucosal T<sub>RM</sub> cell function. The role of CRIP1 expression after successful treatment is similarly unknown. CRIP1 is a zinc-binding protein with high expression in immune cells and epithelium that may play a role in DNA damage repair (Hallquist et al., 1996; Sun et al., 2021; Zhang et al., 2019). Its role in allograft recovery after ACR requires further study.

In addition to small sample size, a limitation to our study is that we have not unequivocally demonstrated that the oligoclonal CD8<sup>+</sup> T cell expansions we detected in the BAL and lung parenchyma during ACR are alloreactive. However, cumulative evidence, including clonal expansion, a type 1/cytotoxic phenotype, and perivascular localization at the time of ACR, strongly suggest alloreactivity. Nonetheless, further studies are required to conclusively demonstrate allospecificity of recipient-

derived T cell that develop into airway-centered, allograft T<sub>RM</sub> cells.

In conclusion, we show that during ACR, the human lung allograft contains a clonally expanded population of recipient-derived CD8<sup>+</sup> T cells that persist as transcriptionally reprogrammed T<sub>RM</sub> cells after systemic therapy with high-dose glucocorticoids.

## Materials and methods

### Study participants

We identified a convenience sample of consecutive adults who underwent a first lung transplantation at the University of Pittsburgh between June 2015 and July 2018, had consented to our institutional review board-approved (STUDY20060250) biorepository, had cryopreserved cells obtained from BAL at the time of ACR and after successful treatment for rejection, and had donor and recipient HLA discrepancies amenable to differentiation with commercially available flow cytometry antibodies (Snyder et al., 2019; Table S2). ACR was defined clinically, as a perivascular infiltration of lymphocytes found on transbronchial biopsy.

### Sample collection, processing, and flow cytometry

BAL samples were centrifuged, and the pellet was reexpanded in FBS with 10% DMSO and frozen in liquid nitrogen for storage. Cells were thawed with warmed medium (RPMI + 10% FBS) and strained sequentially through 100- and 70-mm filters. Samples

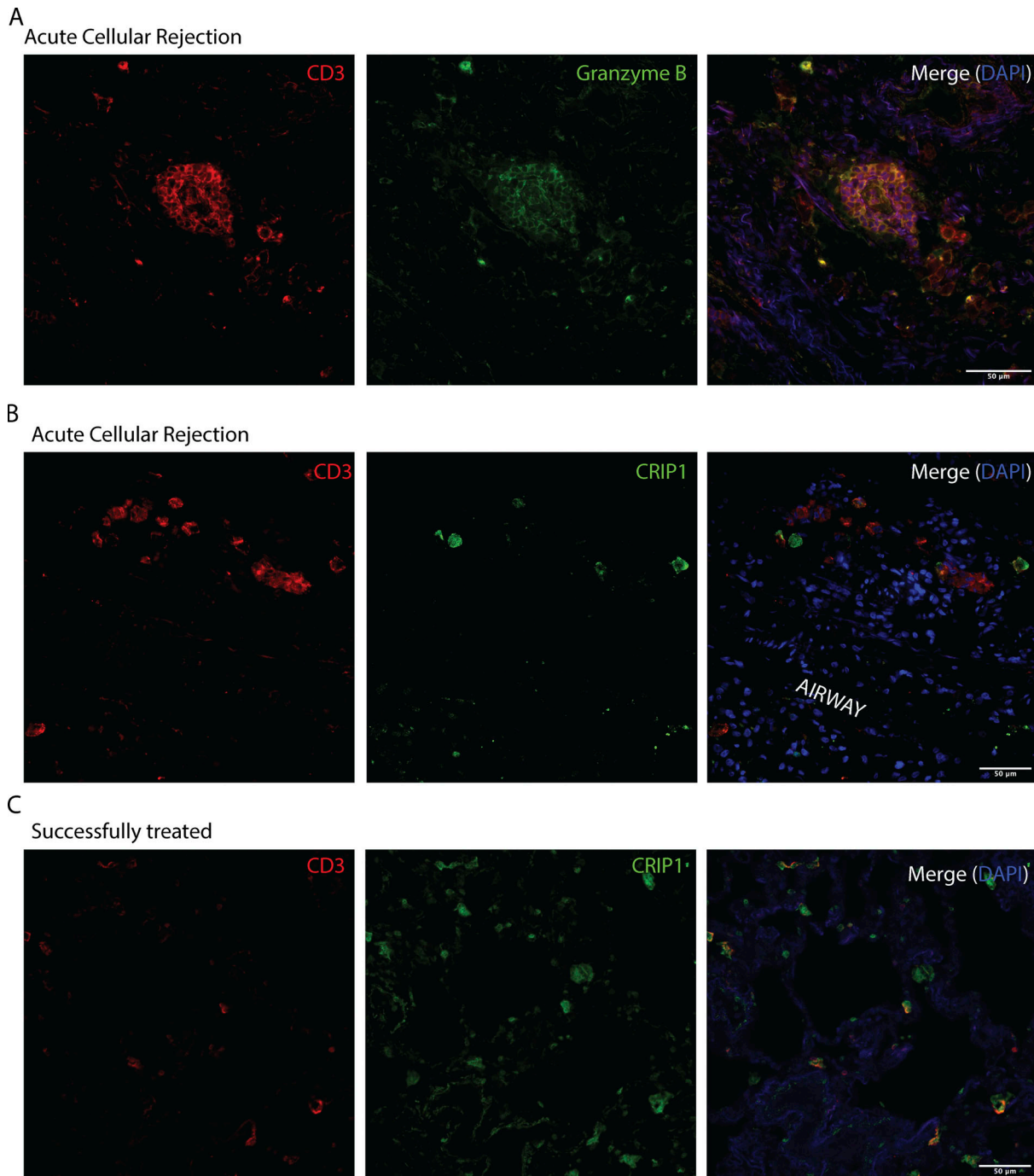


Figure 8. **Anatomic localization of cytotoxic T cells and CRIP1 colocalization after treatment. (A)** Immunofluorescence imaging of CD3 (red) and granzyme B (green) highlighting a perivascular infiltrate of double-positive cells at the time of ACR. **(B)** CRIP1 protein content (green) does not colocalize with CD3 (red) at the time of ACR. **(C)** CRIP1 colocalizes with CD3 (red) after successful treatment with high-dose glucocorticoids.

were then washed with FACS buffer (PBS + 1% FBS) and re-expanded with FACS buffer + 5 mM Fc receptor blocking solution (Human TruStain FcX; BioLegend) for 10 min at room temperature. Afterward, cell surface antibodies were applied at room temperature for 30–60 min and fixed on ice for 60 min (88-8824-00; eBioscience). For panels with intracellular staining, cells were washed with and stained in the presence of a permeabilization buffer. For viral dextramers, we incubated the

cells with dextramer at room temperature for 10 min before adding cell surface stains; panels including dextramers were not fixed before analysis. Flow cytometry was performed using a spectral flow cytometer (CyTek Aurora), and data were analyzed using FlowJo. Methods for distinguishing donor versus recipient origin of immune cells from the BAL has been previously reported (Snyder et al., 2019). All antibodies used for flow cytometry and imaging can be found in Table S3.

### Immunohistochemistry and imaging analysis

5- $\mu$ m sections of paraffin-embedded transbronchial biopsies were obtained from paraffin-embedded blocks maintained by the Pathology Department at the University of Pittsburgh. Slide deparaffinization was performed with >98.5% xylene followed by serial dilutions of ethanol. Antigen retrieval was performed at 95°C for 20 min in the presence of DAKO Target Retrieval Solution, pH 9 (Agilent), using a Decloaking Chamber NxGen (Biocare Medical). Primary antibody was stained overnight on an orbital shaker at 4°C. Secondary antibody was then applied for 1 h on an orbital shaker at room temperature (Table S3 includes list of all antibodies used). Slides were washed and stained with 1 $\times$  DAPI for 5 min. Coverslips were then mounted with ProLong Gold antifade reagent (Invitrogen) and sealed with clear nail polish. Images were captured within 72 h with an epifluorescence microscope (Nikon Eclipse Ni) and a digital camera (Hamamatsu Digital Camera C11440). ImageJ was used to qualitatively analyze images and generate TIFF files from ND2.

### Mixed lymphocyte reaction

Peripheral blood was collected in heparinized BD Vacutainer tubes, and PBMCs were isolated using Ficoll gradient following standard protocols. RPMI supplemented with 35% FBS and 10% DMSO was used to freeze the purified PBMCs in the vapor phase of liquid nitrogen at a density of 5–10  $\times$  10<sup>6</sup> cells per milliliter of medium. Cryopreserved donor PBMCs were thawed, and half were labeled with cell trace dye (CFSE) and  $\gamma$ -irradiated (3,000 rad). The remaining donor PBMCs were lysed using sonication. Single-cell suspensions of BAL obtained at different time points (Fig. 2 A) were stained with cell trace dye (Cell Trace Violet). Irradiated donor PBMCs were combined with single-cell suspensions of labeled BAL cells at a ratio of 1:1, with the simultaneous addition of lysed donor PBMCs in mixed lymphocyte reaction medium (AIM-V with 5% human serum and penicillin/streptomycin/L-glutamine) for 6 h at 37° in a 5% CO<sub>2</sub> incubator (Macedo et al., 2009).

### Single-cell RNAseq/TCR sequencing

Live, recipient-derived CD3<sup>+</sup> T cells were isolated from the BAL using a BD FACSAria (BD Biosciences) sorting on live, CD3<sup>+</sup>, CFSE-negative, irradiated donor PBMC singlets that were positive for recipient-derived HLA. Sorted cells were loaded onto a Chromium Next GEM Single Cell 5' v1 Chip (10x Genomics) according to the manufacturer's guidelines at a capture rate of 5,000 cells per sample. Libraries were sequenced using the Illumina HiSeq 2500 platform. Alignment, filtering, barcode counting, and unique molecular identifier counting were performed with CellRanger v5 and CellRanger VDJ. Quality metrics for each sample can be found in Table S4. Sequencing data are publicly available on GEO (GSE185659).

### Single-cell RNAseq/TCR data processing

Single-cell RNAseq analysis was performed using Seurat v3.0 with R (v3.6). TCR repertoire data were embedded in the Seurat object metadata using scRepertoire (Koch et al., 2018). Normalization and variance stabilization of count data were performed using scTransform (Hafemeister and Satija, 2019).

Seurat objects were then integrated using 3,000 identified anchors based on the previously transformed normalization values. A small number of contaminating cells of myeloid descent were removed from analyses based on CD68 expression, followed by spatial visualization of distinct clusters using UMAP for dimension reduction (Becht et al., 2018). For differential expression analysis between ACR and treatment, data was divided to include only the top four clones present at the time of rejection. Differential gene expression was performed from this subset using nonparametric Wilcoxon rank-sum test. The results were adjusted for multiple comparisons using Bonferroni correction. All code used for single-cell analyses can be found in the following GitHub repository, including a list of all R packages used for analyses: [https://github.com/markesnyder/LTX\\_scACR](https://github.com/markesnyder/LTX_scACR).

### Bulk TCR sequencing and analysis

Peripheral blood was collected longitudinally from lung transplant recipients as part of our ongoing transplant biorepository. Lymphocytes were isolated using density centrifugation with lymphocyte separation medium (Corning LSM). Lymphocytes were then slowly cryopreserved in FBS with 10% dimethyl sulfoxide and stored in the vapor phase of liquid nitrogen. Samples identified for study use were slowly thawed. Genomic DNA was isolated from FACS-sorted, recipient-derived circulating T cells (either alloreactive or unstimulated) using DNeasy Blood & Tissue Kit (Qiagen). Unstimulated T cells were derived from FACS sorting live, CD3<sup>+</sup>, recipient HLA<sup>+</sup> lymphocytes; alloreactive T cells were isolated by sorting CD8<sup>+</sup> and CD4<sup>+</sup> recipient HLA<sup>+</sup> lymphocytes that were positive for activation-induced markers (AIMs) after 12-h stimulation with irradiated donor PBMCs (Reiss et al., 2017). Positivity for AIM markers after mixed lymphocyte reaction was defined as CD69<sup>+</sup> and/or CD137<sup>+</sup> for CD8<sup>+</sup> T cells and CD69<sup>+</sup> and/or OX40<sup>+</sup> for CD4<sup>+</sup> T cells (Fig. S5 A). The gating strategy for sorting was established based on AIM marker expression of resting T cells in the absence of ACR (Fig. S5 B). At the time of ACR, there were a substantial number of CD69<sup>+</sup> recipient CD3<sup>+</sup> T cells at rest (Fig. S5 C). DNA was quantified with NanoDrop One (Thermo Fisher Scientific). Next-generation TCR  $\beta$  sequencing of CDR3 variable region was performed using the ImmunoSeq hsTCRBkit (Adaptive Biotechnologies) and sequenced with a MiSeq 150 $\times$  system (Illumina). Data was analyzed using both the ImmunoSeq Analyzer software v3.0 (Adaptive Biotechnologies; DeWitt et al., 2015; Rytlewski et al., 2019) and Immunarch (Nazarov et al., 2020).

### T cell repertoire diversity

T cell repertoire diversity within the BAL at the time of ACR and after treatment was estimated via multiple indices. The Shannon index assumes that all clones are represented in the sample and that these clones have been randomly selected:

$$-\sum_{i=1}^c \frac{n}{N} \ln \frac{n}{N},$$

where  $c$  = the number of distinct clones, and  $\frac{n}{N}$  is the proportion of an individual clone ( $n$ ) over clonal abundance ( $N$ ).

The inverse Simpson index places more weight on dominant clones:

$$\frac{1}{\left(1 - \sum_{i=1}^c \left(\frac{n_i}{N}\right)^2\right)}$$

The Chao1-index focuses on clonal abundance, including only those clones with one or two copies:

$$c + a_1(a_1 - 1) / (2a_2 + 1),$$

where  $a_1$  is the number of single clones, and  $a_2$  is the number of clones with two copies.

The abundance-based coverage estimator is another index of clonal richness, like Chao1, but focusing on all clones with  $\leq 10$  copies each (instead of just one or two copies):

$$\sum_{i=1}^c p_i I(N_i > 0),$$

where  $p_i = \frac{N_i}{N}$ , and  $I(A)$  is the indicator function (Chao and Chiu, 2014).

### TCR viral specificity

10× VDJ files were read using Immunarch package in R. The VDJdb database (Shugay et al., 2018) of HLA-conserved, viral-specific CDR3 amino acid sequences was downloaded from <https://gitlab.com/immunomind/immunarch/raw/dev-0.5.0/private/vdjdbc.slim.txt.gz>. The database was filtered for .species = “HomoSapiens,” .chain = “TCRB,” and pathology = c (“InfluenzaA,” “CMV,” “EBV”). We cross-referenced CDR3.aa from the TCR  $\beta$  of CellRanger VDJ output with that of the VDJdb database and kept HLA-conserved matches. Results were visualized using ggplot2.

### RNA in situ hybridization assay (BaseScope)

Transbronchial biopsy slides underwent deparaffinization, rehydration, and antigen retrieval as described in Immunohistochemistry and imaging analysis. Slides were pretreated with protease. We had two probes designed to bind to the hyper-variable CDR3- $\beta$  segment of our most abundant clone in participants P1 and P8 at the time of ACR; probes were hybridized to our target mRNA and amplified per the manufacturer’s instructions. Slides were counterstained with 50% hematoxylin solution, washed with tap water, immersed in 0.02% ammonia water, and again washed with tap water before mounting. Images were captured at both 40× and 60× magnification using a Nikon Eclipse Ni and a digital camera (Hamamatsu Digital Camera C11440). Whole slides were scanned at 40× using a Zeiss Axio Scan.Z1, and positively stained cells were manually counted and determined to be close to the airways if they were within the intra-epithelial, subepithelial, or peribronchiolar regions of the lung.

### Statistical analysis

Statistical analyses were performed using R (R Foundation for statistical computing), Python (Python Software Foundation), and GraphPad (Prism). For all analyses, a two-tailed P value of  $<0.05$  was the threshold used to determine statistical

significance. Immunohistochemistry and immunofluorescence were analyzed with ImageJ. Paired *t* test was used to test for difference in flow cytometry T cell phenotype before, during, and after ACR. Figures were compiled using Adobe Illustrator CC 2017.

### Online supplemental material

Fig. S1 shows a representative flow cytometry plot demonstrating the gating strategy to differentiate donor versus recipient-derived T cells from the BAL of lung transplant recipients by staining for unique HLAs. Fig. S2 shows clonal diversity of TCR repertoire at different time points using a variety of metrics, as well as clonal distribution by RNA clustering. Fig. S3 shows the representative images of BaseScope for study participant P8. Fig. S4 shows the flow cytometry tSNE distributed by study participant as well as representative immunofluorescence imaging of CD3 and granzyme B of transbronchial biopsies. Fig. S5 presents representative sorting gates for isolating circulating recipient T cells using FACS sorting. Table S1 presents the results of TCR specificity analysis using GLIPH. Table S2 displays the study participant HLA for both donor and recipient. Table S3 catalogues all antibodies used for analyses. Table S4 presents the quality matrix values for single-cell files used in this analysis.

### Data availability

Raw data were generated at the University of Pittsburgh and are included in the article and supplementary materials. The complete set of raw data supporting the findings of this study are available from the corresponding author, M.E. Snyder, on request.

### Acknowledgments

The authors would like to thank K. Abou-Daya at the University of Pittsburgh for guidance with single-cell analysis, D. Metes at the University of Pittsburgh for guidance with mixed lymphocyte reactions, and F. Lakkis at the University of Pittsburgh for guidance and feedback. As always, a special thanks to the families of organ donors who made transplantation possible.

This work was supported by National Institutes of Health K23 HL151750-01 awarded to M.E. Snyder and 1R01HL133184 awarded to J.F. McDyer.

Author contributions: M.E. Snyder, A. Bondonese, and A. Craig performed experiments. R. Lafyatis and T. Tabib oversaw and performed cell capture and library preparation for single-cell RNA and TCR sequencing. K. Chen and I. Popescu oversaw and performed read quality control and alignment. E. Lendermon, J. Pilewski, B. Johnson, S. Kilaru, and P.G. Sanchez assisted in sample acquisition. Y. Zhang oversaw sample storage and retrieval. H.E. Trejo Bittar assisted with pathology review. M.E. Snyder and K. Moghbeli analyzed single-cell RNA/TCR and bulk TCR data with the guidance of P.A. Sims. J.K. Alder assisted with RNA in situ hybridization and with imaging analysis. L. Fan, P.A. Sims, and J.F. McDyer supervised the work and guided

design. All authors provided a critical review of the manuscript and assisted with revisions.

Disclosures: R. Lafyatis reported grants from Moderna, Corbus, Formation, Regeneron, Astra Zeneca, Pfizer, Kiniksa, and Mitsubishi; and personal fees from Pfizer, Boehringer-Ingelheim, Sanofi, Boehringer-Mannheim, Merck, Biogen, Genentech, and Bristol Myers Squibb outside the submitted work. J. Pilewski reported grants from Breath Therapeutics and Incyte outside the submitted work. J.K. Alder reported grants from National Heart, Lung, and Blood Institute during the conduct of the study. No other disclosures were reported.

Submitted: 4 October 2021

Revised: 13 December 2021

Accepted: 4 February 2022

## References

- Abou-Daya, K.I., R. Tieu, D. Zhao, R. Rammal, F. Sacirbegovic, A.L. Williams, W.D. Shlomchik, M.H. Oberbarnscheidt, and F.G. Lakkis. 2021. Resident memory T cells form during persistent antigen exposure leading to allograft rejection. *Sci. Immunol.* 6:eabc8122. <https://doi.org/10.1126/sciimmunol.abc8122>
- Alachkar, H., M. Mutonga, T. Kato, S. Kalluri, Y. Kakuta, M. Uemura, R. Imamura, N. Nonomura, V. Vujjini, S. Alasfar, H. Rabb, et al. 2016. Quantitative characterization of T-cell repertoire and biomarkers in kidney transplant rejection. *BMC Nephrol.* 17:181. <https://doi.org/10.1186/s12882-016-0395-3>
- Alegre, M.-L., F.G. Lakkis, and A.E. Morelli. 2016. Antigen presentation in transplantation. *Trends Immunol.* 37:831–843. <https://doi.org/10.1016/j.it.2016.09.003>
- Becht, E., L. McInnes, J. Healy, C.-A. Dutertre, I.W.H. Kwok, L.G. Ng, F. Ginhoux, and E.W. Newell. 2018. Dimensionality reduction for visualizing single-cell data using UMAP. *Nat. Biotechnol.* 37:38–44. <https://doi.org/10.1038/nbt.4314>
- Bereshchenko, O., M. Coppo, S. Bruscoli, M. Biagioli, M. Cimino, T. Frammartino, D. Sorcini, A. Venanzi, M. Di Sante, and C. Riccardi. 2014. GILZ promotes production of peripherally induced Treg cells and mediates the crosstalk between glucocorticoids and TGF- $\beta$  signaling. *Cell Rep.* 7: 464–475. <https://doi.org/10.1016/j.celrep.2014.03.004>
- Cepek, K.L., S.K. Shaw, C.M. Parker, G.J. Russell, J.S. Morrow, D.L. Rimm, and M.B. Brenner. 1994. Adhesion between epithelial cells and T lymphocytes mediated by E-cadherin and the alpha E beta 7 integrin. *Nature.* 372:190–193. <https://doi.org/10.1038/372190a0>
- Chao, A., and C.-H. Chiu. 2014. Species richness: estimation and comparison. In *Wiley Statsref: Statistics Reference Online*. N.Balakrishnan, T. Colton, B. Everitt, W. Piegorisch, F. Ruggeri, and J.L. Teugels, editors. John Wiley & Sons, Ltd, Chichester, UK. 1–26.
- Clark, R.A., R. Watanabe, J.E. Teague, C. Schlapbach, M.C. Tawa, N. Adams, A.A. Dorosario, K.S. Chaney, C.S. Cutler, N.R. Leboeuf, J.B. Carter, et al. 2012. Skin effector memory T cells do not recirculate and provide immune protection in alemtuzumab-treated CTCL patients. *Sci. Transl. Med.* 4:117ra7. <https://doi.org/10.1126/scitranslmed.3003008>
- Clelland, C.A., T.W. Higebottom, S. Stewart, J.P. Scott, and J. Wallwork. 1990. The histological changes in transbronchial biopsy after treatment of acute lung rejection in heart-lung transplants. *J. Pathol.* 161:105–112. <https://doi.org/10.1002/path.1711610204>
- de Leur, K., M. Dieterich, D.A. Hesselink, O.B.J. Corneth, F.J.M.F. Dor, G.N. de Graav, A.M.A. Peeters, A. Mulder, H.J.A.N. Kimenai, F.H.J. Claas, M.C. Clahsen-van Groningen, et al. 2019. Characterization of donor and recipient CD8<sup>+</sup> tissue-resident memory T cells in transplant nephrectomies. *Sci. Rep.* 9:5984. <https://doi.org/10.1038/s41598-019-42401-9>
- DeWitt, W.S., R.O. Emerson, P. Lindau, M. Vignali, T.M. Snyder, C. Desmarais, C. Sanders, H. Utsugi, E.H. Warren, J. McElrath, K.W. Makar, et al. 2015. Dynamics of the cytotoxic T cell response to a model of acute viral infection. *J. Virol.* 89:4517–4526. <https://doi.org/10.1128/JVI.03474-14>
- Glanville, J., H. Huang, A. Nau, O. Hatton, L.E. Wagar, F. Rubelt, X. Ji, A. Han, S.M. Krams, C. Pettus, N. Haas, et al. 2017. Identifying specificity groups in the T cell receptor repertoire. *Nature.* 547:94–98. <https://doi.org/10.1038/nature22976>
- Gullberg, D., K.R. Gehlsen, D.C. Turner, K. Ahlén, L.S. Zijenah, M.J. Barnes, and K. Rubin. 1992. Analysis of alpha 1 beta 1, alpha 2 beta 1 and alpha 3 beta 1 integrins in cell-collagen interactions: identification of conformation dependent alpha 1 beta 1 binding sites in collagen type I. *EMBO J.* 11:3865–3873
- Hafemeister, C., and R. Satija. 2019. Normalization and variance stabilization of single-cell RNA-seq data using regularized negative binomial regression. *Genome Biol.* 20:296. <https://doi.org/10.1186/s13059-019-1874-1>
- Hallquist, N.A., C. Khoo, and R.J. Cousins. 1996. Lipopolysaccharide regulates cysteine-rich intestinal protein, a zinc-finger protein, in immune cells and plasma. *J. Leukoc. Biol.* 59:172–177. <https://doi.org/10.1002/jlb.59.2.172>
- Hughes, A.D., D. Zhao, H. Dai, K.I. Abou-Daya, R. Tieu, R. Rammal, A.L. Williams, D.P. Landsittel, W.D. Shlomchik, A.E. Morelli, M.H. Oberbarnscheidt, et al. 2020. Cross-dressed dendritic cells sustain effector T cell responses in islet and kidney allografts. *J. Clin. Invest.* 130:287–294. <https://doi.org/10.1172/JCI125773>
- Iasella, C.J., A. Hoji, I. Popescu, J. Wei, M.E. Snyder, Y. Zhang, W. Xu, V. Iouchmanov, R. Koshy, M. Brown, M. Fung, et al. 2021. Type-1 immunity and endogenous immune regulators predominate in the airway transcriptome during chronic lung allograft dysfunction. *Am. J. Transpl.* 21:2145–2160. <https://doi.org/10.1111/ajt.16360>
- Koch, H., D. Starenki, S.J. Cooper, R.M. Myers, and Q. Li. 2018. powerTCR: a model-based approach to comparative analysis of the clone size distribution of the T cell receptor repertoire. *PLoS Comput. Biol.* 14: e1006571. <https://doi.org/10.1371/journal.pcbi.1006571>
- Kumar, B.V., W. Ma, M. Miron, T. Granot, R.S. Guyer, D.J. Carpenter, T. Senda, X. Sun, S.-H. Ho, H. Lerner, A.L. Friedman, et al. 2017. Human tissue-resident memory T cells are defined by core transcriptional and functional signatures in lymphoid and mucosal sites. *Cell Rep.* 20: 2921–2934. <https://doi.org/10.1016/j.celrep.2017.08.078>
- Levine, S.M., and Transplant/Immunology Network of the American College of Chest Physicians. 2004. A survey of clinical practice of lung transplantation in North America. *Chest.* 125:1224–1238. <https://doi.org/10.1378/chest.125.4.1224>
- Macedo, C., E.A. Orkis, I. Popescu, B.D. Elinoff, A. Zeevi, R. Shapiro, F.G. Lakkis, and D. Metes. 2009. Contribution of naïve and memory T-cell populations to the human alloimmune response. *Am. J. Transpl.* 9: 2057–2066. <https://doi.org/10.1111/j.1600-6143.2009.02742.x>
- Mahata, B., X. Zhang, A.A. Kolodziejczyk, V. Proserpio, L. Haim-Vilmsky, A.E. Taylor, D. Hebenstreit, F.A. Dingler, V. Moignard, B. Göttgens, W. Arlt, et al. 2014. Single-cell RNA sequencing reveals T helper cells synthesizing steroids de novo to contribute to immune homeostasis. *Cell Rep.* 7:1130–1142. <https://doi.org/10.1016/j.celrep.2014.04.011>
- Marino, J., J. Paster, and G. Benichou. 2016. Allorecognition by T Lymphocytes and allograft rejection. *Front. Immunol.* 7:582. <https://doi.org/10.3389/fimmu.2016.00582>
- Martinu, T., D.-F. Chen, and S.M. Palmer. 2009. Acute rejection and humoral sensitization in lung transplant recipients. *Proc. Am. Thorac. Soc.* 6: 54–65. <https://doi.org/10.1513/pats.200808-080GO>
- Martinu, T., E.N. Pavlisko, D.-F. Chen, and S.M. Palmer. 2011. Acute allograft rejection: cellular and humoral processes. *Clin. Chest Med.* 32:295–310. <https://doi.org/10.1016/j.ccm.2011.02.008>
- Migita, K., K. Eguchi, Y. Kawabe, T. Nakamura, S. Shirabe, T. Tsukada, Y. Ichinose, H. Nakamura, and S. Nagataki. 1997. Apoptosis induction in human peripheral blood T lymphocytes by high-dose steroid therapy. *Transplantation.* 63:583–587. <https://doi.org/10.1097/00007890-199702270-00017>
- Moser, J.M., J. Gibbs, P.E. Jensen, and A.E. Lukacher. 2002. CD94-NKG2A receptors regulate antiviral CD8(+) T cell responses. *Nat. Immunol.* 3: 189–195. <https://doi.org/10.1038/ni757>
- Nazarov, V., and E. Rumynskiy; Immunarch.Bot. 2020. immunomind/immunarch: 0.5.5 (0.5.5). *Zenodo.* <https://doi.org/10.5281/zenodo.3613560>
- Oja, A.E., B. Piet, C. Helbig, R. Stark, D. van der Zwan, H. Blaauwgeers, E.B.M. Remmerswaal, D. Amsen, R.E. Jonkers, P.D. Moerland, M.A. Nolte, et al. 2018. Trigger-happy resident memory CD4<sup>+</sup> T cells inhabit the human lungs. *Mucosal Immunol.* 11:654–667. <https://doi.org/10.1038/mi.2017.94>
- Paliogianni, F., S.S. Ahuja, J.P. Balow, J.E. Balow, and D.T. Boumpas. 1993. Novel mechanism for inhibition of human T cells by glucocorticoids. Glucocorticoids inhibit signal transduction through IL-2 receptor. *J. Immunol.* 151:4081–4089.
- Park, S.L., A. Zaid, J.L. Hor, S.N. Christo, J.E. Prier, B. Davies, Y.O. Alexandre, J.L. Gregory, T.A. Russell, T. Gebhardt, F.R. Carbone, et al. 2018. Local proliferation maintains a stable pool of tissue-resident memory T cells

- after antiviral recall responses. *Nat. Immunol.* 19:183–191. <https://doi.org/10.1038/s41590-017-0027-5>
- Reams, B.D., L.W. Musselwhite, D.W. Zaas, M.P. Steele, S. Garantziotis, P.C. Eu, L.D. Snyder, J. Curl, S.S. Lin, R.D. Davis, and S.M. Palmer. 2007. Alem-tuzumab in the treatment of refractory acute rejection and bronchiolitis obliterans syndrome after human lung transplantation. *Am. J. Transpl.* 7: 2802–2808. <https://doi.org/10.1111/j.1600-6143.2007.02000.x>
- Reilly, E.C., K. Lambert Emo, P.M. Buckley, N.S. Reilly, I. Smith, F.A. Chaves, H. Yang, P.W. Oakes, and D.J. Topham. 2020. T<sub>RM</sub> integrins CD103 and CD49a differentially support adherence and motility after resolution of influenza virus infection. *Proc. Natl. Acad. Sci. USA.* 117:12306–12314. <https://doi.org/10.1073/pnas.1915681117>
- Reiss, S., A.E. Baxter, K.M. Cirelli, J.M. Dan, A. Morou, A. Daigneault, N. Brassard, G. Silvestri, J.-P. Routy, C. Havenar-Daughton, S. Crotty, et al. 2017. Comparative analysis of activation induced marker (AIM) assays for sensitive identification of antigen-specific CD4 T cells. *PLoS One.* 12: e0186998. <https://doi.org/10.1371/journal.pone.0186998>
- Rytlewski, J., S. Deng, T. Xie, C. Davis, H. Robins, E. Yusko, and J. Bienkowska. 2019. Model to improve specificity for identification of clinically-relevant expanded T cells in peripheral blood. *PLoS One.* 14:e0213684. <https://doi.org/10.1371/journal.pone.0213684>
- Schenkel, J.M., and D. Masopust. 2014. Tissue-resident memory T cells. *Im-munity.* 41:886–897. <https://doi.org/10.1016/j.immuni.2014.12.007>
- Shugay, M., D.V. Bagaev, I.V. Zvyagin, R.M. Vroomans, J.C. Crawford, G. Dolton, E.A. Komech, A.L. Sycheva, A.E. Koneva, E.S. Egorov, A.V. Eli-seev, et al. 2018. VDJdb: a curated database of T-cell receptor sequences with known antigen specificity. *Nucleic Acids Res.* 46:D419–D427. <https://doi.org/10.1093/nar/gkx760>
- Skon, C.N., J.-Y. Lee, K.G. Anderson, D. Masopust, K.A. Hogquist, and S.C. Jameson. 2013. Transcriptional downregulation of Slpr1 is required for the establishment of resident memory CD8<sup>+</sup> T cells. *Nat. Immunol.* 14: 1285–1293. <https://doi.org/10.1038/ni.2745>
- Snyder, M.E., M.O. Finlayson, T.J. Connors, P. Dogra, T. Senda, E. Bush, D. Carpenter, C. Marboe, L. Benvenuto, L. Shah, H. Robbins, et al. 2019. Generation and persistence of human tissue-resident memory T cells in lung transplantation. *Sci. Immunol.* 4:eaav5581. <https://doi.org/10.1126/sciimmunol.aav5581>
- Snyder, M.E., J. Sembrat, K. Noda, M.M. Myerburg, A. Craig, N. Mitash, T. Harano, M. Furukawa, J. Pilewski, J. McDyer, et al. 2021. Human Lung-Resident Macrophages Colocalize with and Provide Costimulation to PD1<sup>hi</sup> Tissue-Resident Memory T Cells. *Am. J. Respir. Crit. Care Med.* 203: 1230–1244. <https://doi.org/10.1164/rccm.202006-2403OC>
- Snyder, M.E., A. Bondonese, A. Craig, I. Popescu, M.R. Morrell, M.M. Myerburg, C. Iasella, E. Lendermon, J. Pilweski, B. Johnson, et al. 2022. Rate of recipient-derived alveolar macrophage development and major histocompatibility complex cross-decoration after lung transplantation in humans. *Am. J. Transpl.* 22:574–587. <https://doi.org/10.1111/ajt.16812>
- Stranavova, L., O. Pelak, M. Svaton, P. Hrubá, E. Fronková, A. Slavcev, K. Osicková, J. Malusková, P. Hubáček, J. Fronek, P. Reinke, et al. 2019. Heterologous cytomegalovirus and allo-reactivity by shared T cell receptor repertoire in kidney transplantation. *Front. Immunol.* 10:2549. <https://doi.org/10.3389/fimmu.2019.02549>
- Strauch, U.G., R.C. Mueller, X.Y. Li, M. Cernadas, J.M. Higgins, D.G. Binion, and C.M. Parker. 2001. Integrin alpha E(CD103)beta 7 mediates adhesion to intestinal microvascular endothelial cell lines via an E-cadherin-independent interaction. *J. Immunol.* 166:3506–3514. <https://doi.org/10.4049/jimmunol.166.5.3506>
- Sun, H., R. Zhou, Y. Zheng, Z. Wen, D. Zhang, D. Zeng, J. Wu, Z. Huang, X. Rong, N. Huang, L. Sun, et al. 2021. CRIP1 cooperates with BRCA2 to drive the nuclear enrichment of RAD51 and to facilitate homologous repair upon DNA damage induced by chemotherapy. *Oncogene.* 40: 5342–5355. <https://doi.org/10.1038/s41388-021-01932-0>
- Thome, J.J.C., N. Yudanin, Y. Ohmura, M. Kubota, B. Grinshpun, T. Sathaliyawala, T. Kato, H. Lerner, Y. Shen, and D.L. Farber. 2014. Spatial map of human T cell compartmentalization and maintenance over decades of life. *Cell.* 159:814–828. <https://doi.org/10.1016/j.cell.2014.10.026>
- Tickotsky, N., T. Sagiv, J. Prilusky, E. Shifrut, and N. Friedman. 2017. McPAS-TCR: a manually curated catalogue of pathology-associated T cell receptor sequences. *Bioinformatics.* 33:2924–2929. <https://doi.org/10.1093/bioinformatics/btx286>
- Wakim, L.M., and M.J. Bevan. 2011. Cross-dressed dendritic cells drive memory CD8<sup>+</sup> T-cell activation after viral infection. *Nature.* 471: 629–632. <https://doi.org/10.1038/nature09863>
- Weigt, S.S., X. Wang, V. Palchevskiy, X. Li, N. Patel, D.J. Ross, J. Reynolds, P.D. Shah, L.A. Danziger-Isakov, S.C. Sweet, L.G. Singer, et al. 2019. Usefulness of gene expression profiling of bronchoalveolar lavage cells in acute lung allograft rejection. *J. Heart Lung Transpl.* 38:845–855. <https://doi.org/10.1016/j.healun.2019.05.001>
- Yusen, R.D., L.B. Edwards, A.Y. Kucheryavaya, C. Benden, A.I. Dipchand, S.B. Goldfarb, B.J. Levvey, L.H. Lund, B. Meiser, J.W. Rossano, and J. Stehlik. 2015. The registry of the international society for heart and lung transplantation: thirty-second official adult lung and heart-lung transplantation report-2015; focus theme: early graft failure. *J. Heart Lung Transpl.* 34:1264–1277. <https://doi.org/10.1016/j.healun.2015.08.014>
- Zhang, L., R. Zhou, W. Zhang, X. Yao, W. Li, L. Xu, X. Sun, and L. Zhao. 2019. Cysteine-rich intestinal protein 1 suppresses apoptosis and chemo-sensitivity to 5-fluorouracil in colorectal cancer through ubiquitin-mediated Fas degradation. *J. Exp. Clin. Cancer Res.* 38:120. <https://doi.org/10.1186/s13046-019-1117-z>

## Supplemental material

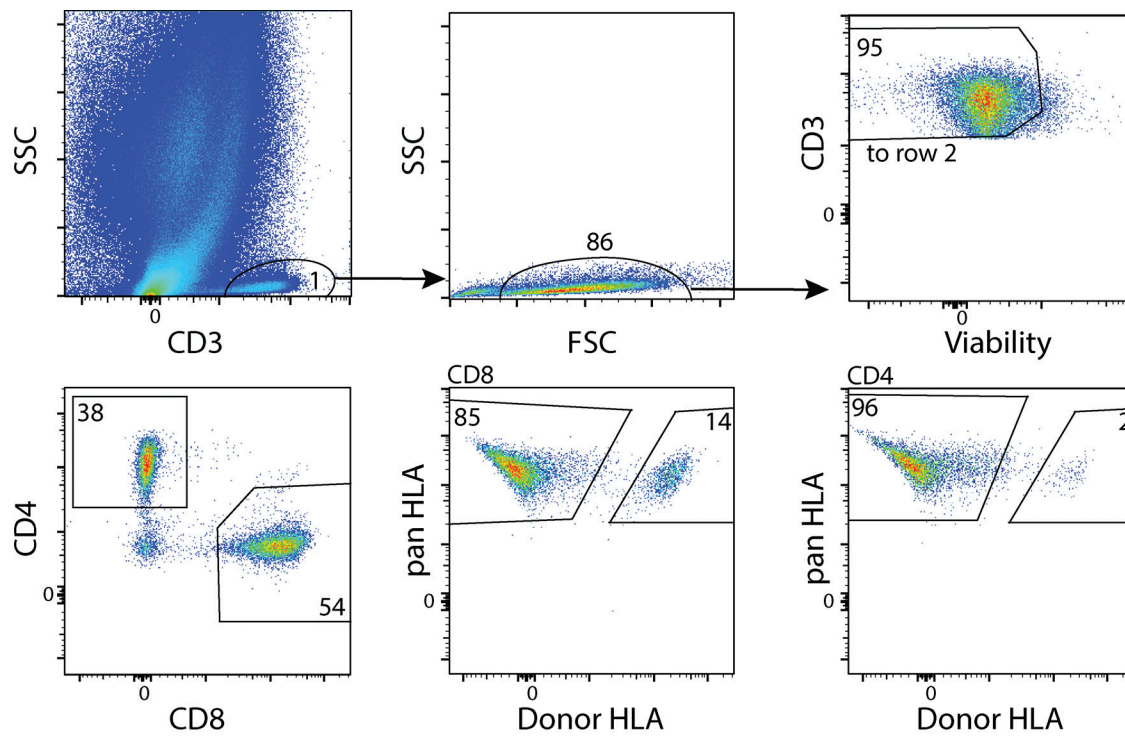


Figure S1. **Donor vs. recipient T cells by flow cytometry.** Representative flow cytometry gating strategy for isolation of donor and recipient T cells from the BAL of lung transplant recipients using HLA discrepancies. FSC, forward scatter; SSC, side scatter.

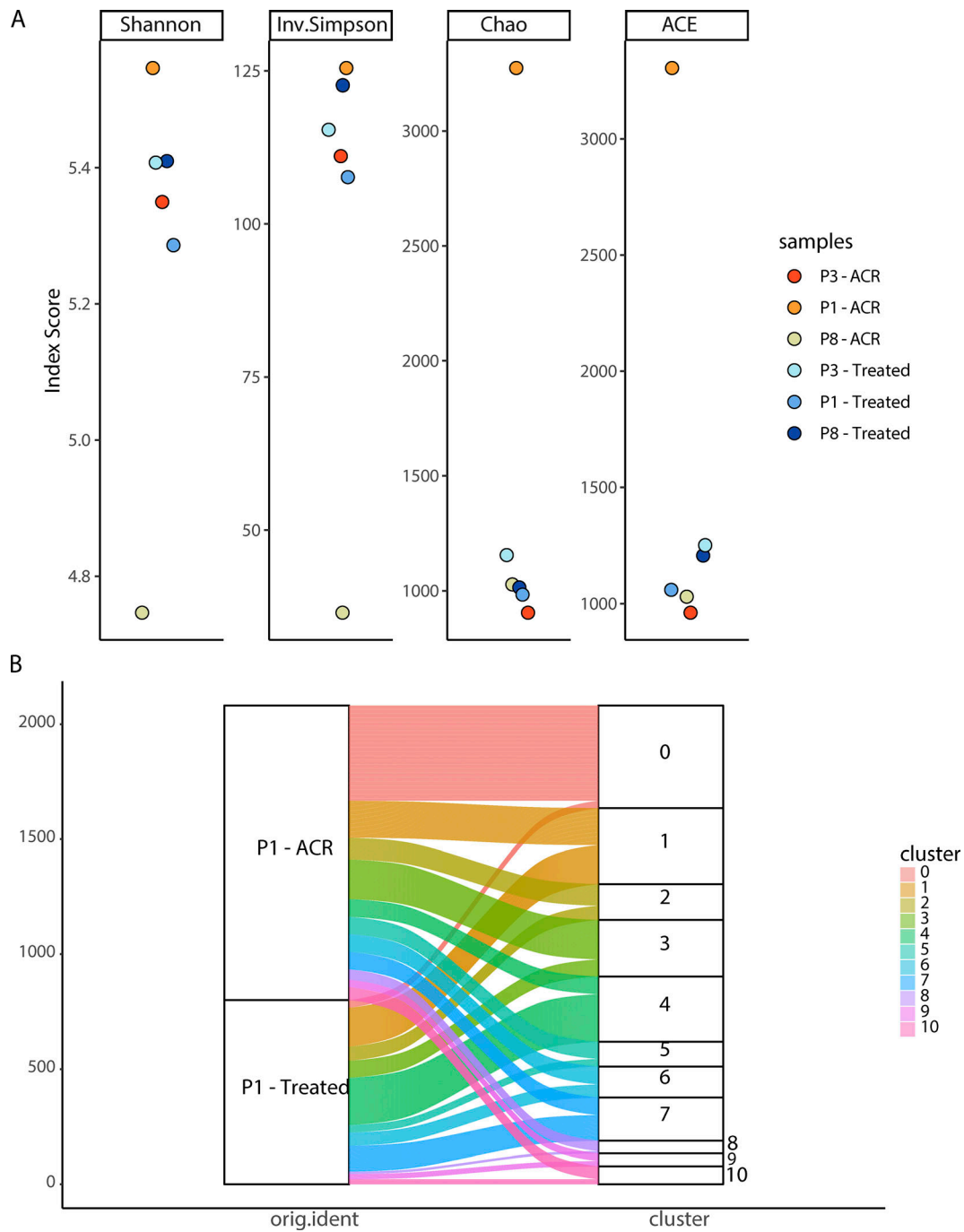


Figure S2. **Oligoclonal expansion of recipient T cells in BAL. (A)** Comparing TCR repertoire diversity, using four different metrics, from three samples at the time of ACR and three samples after treatment. Shannon, Shannon index; Inv.Simpson, inverse Simpson index; Chao, Chao1 index; ACE, abundance-based coverage estimator. **(B)** T cell clonal overlap by presence of ACR or treatment and UMAP cluster. Graph includes only those clones that persisted at the time of treatment.

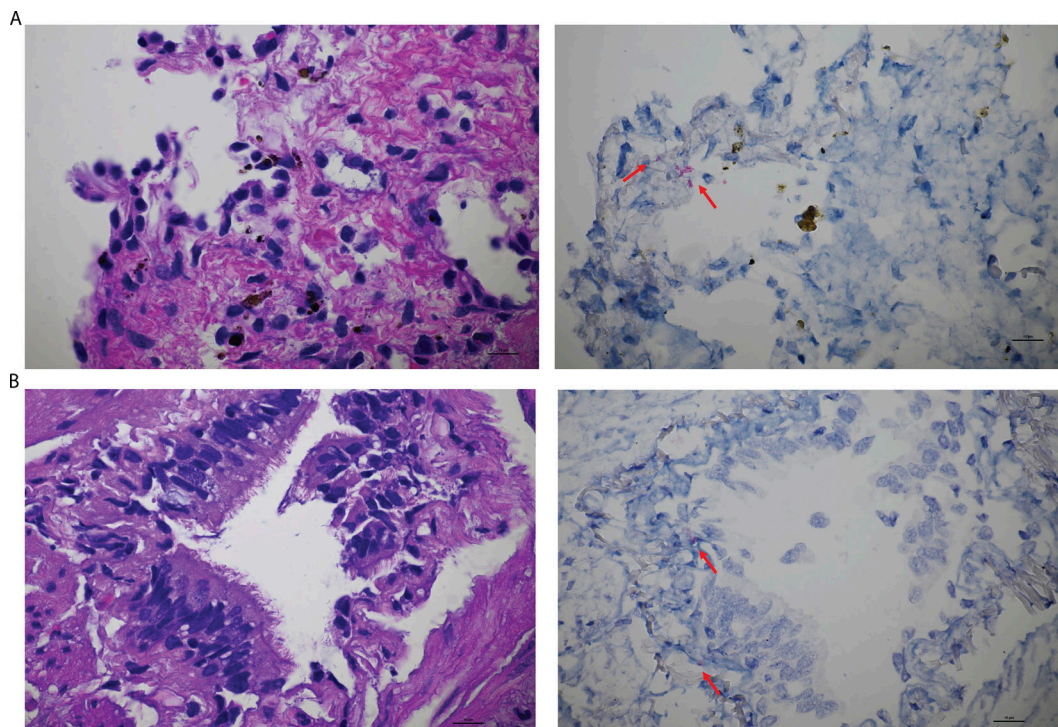


Figure S3. **BaseScope for study participant P8.** (A) H&E stain of transbronchial biopsy of study participant P8 at the time of ACR (left) and RNA in situ hybridization (right, BaseScope), highlighting the parenchymal presence of the top expanded clone found in the BAL at the time of ACR. Red arrows highlight positive staining (red dots). (B) H&E stain of transbronchial biopsy of study participant P8 after successful treatment of ACR (left) and RNA in situ hybridization (right, BaseScope), highlighting the intraepithelial and subepithelial (arrows) presence of the top expanded clone found in the BAL at the time of ACR.

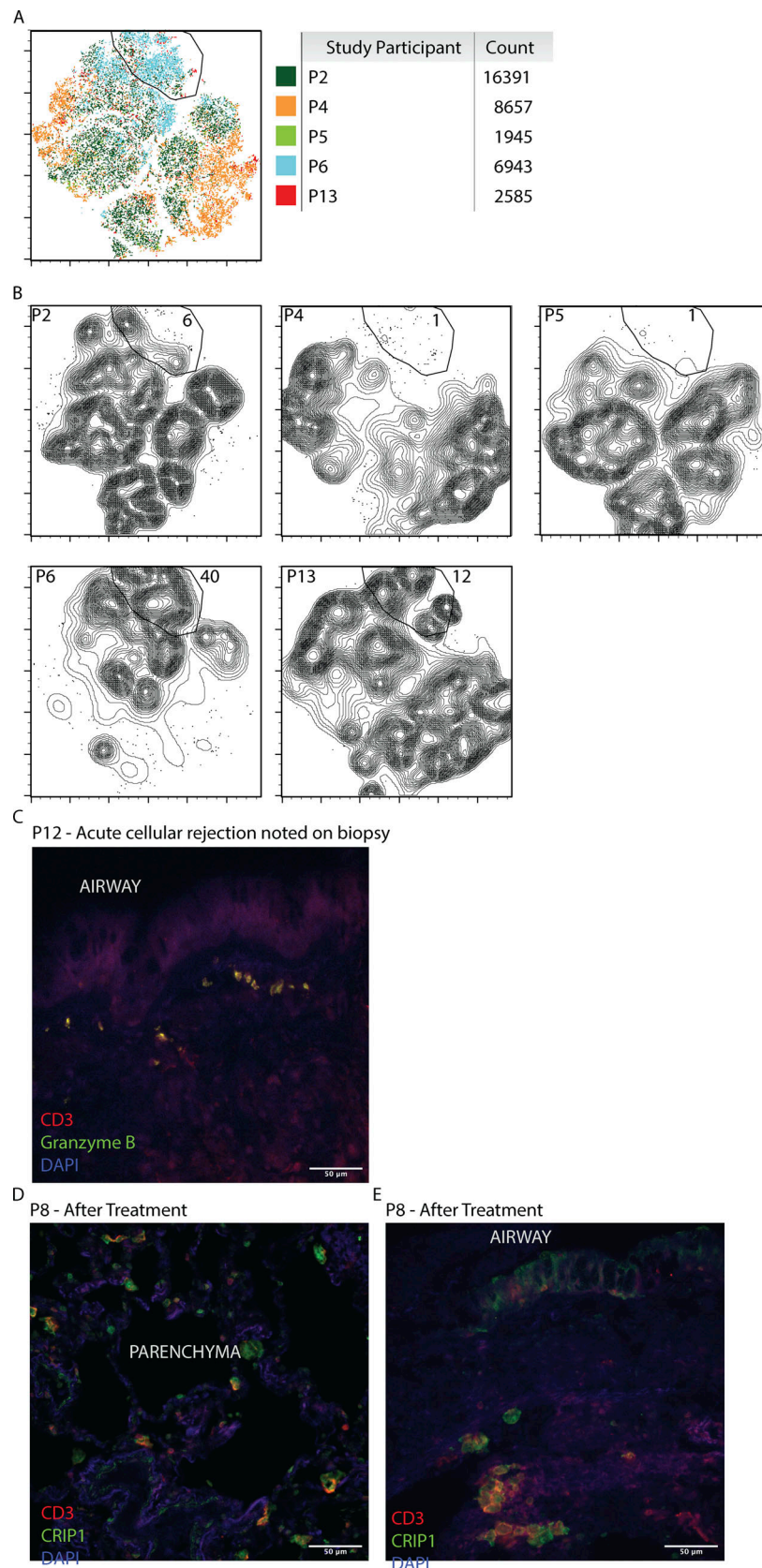


Figure S4. **Flow cytometry tSNE per study participant.** (A) tSNE of concatenated flow cytometry from Fig. 7 indicating patient source, with table showing cell counts per study participant. (B) Contour plot of Fig. 7 divided by study participant, highlighting the percentage of cells within the ACR-specific cluster. (C-E) Multiplex immunofluorescence imaging of transbronchial biopsies for CD3 (red), granzyme B (green), and DAPI (blue) for study participant P12 at the time of ACR (C) and CD3 (red), CRIP1 (green), and DAPI (blue) for study participant P8, including biopsy of the lung parenchyma (D) and airway (E).

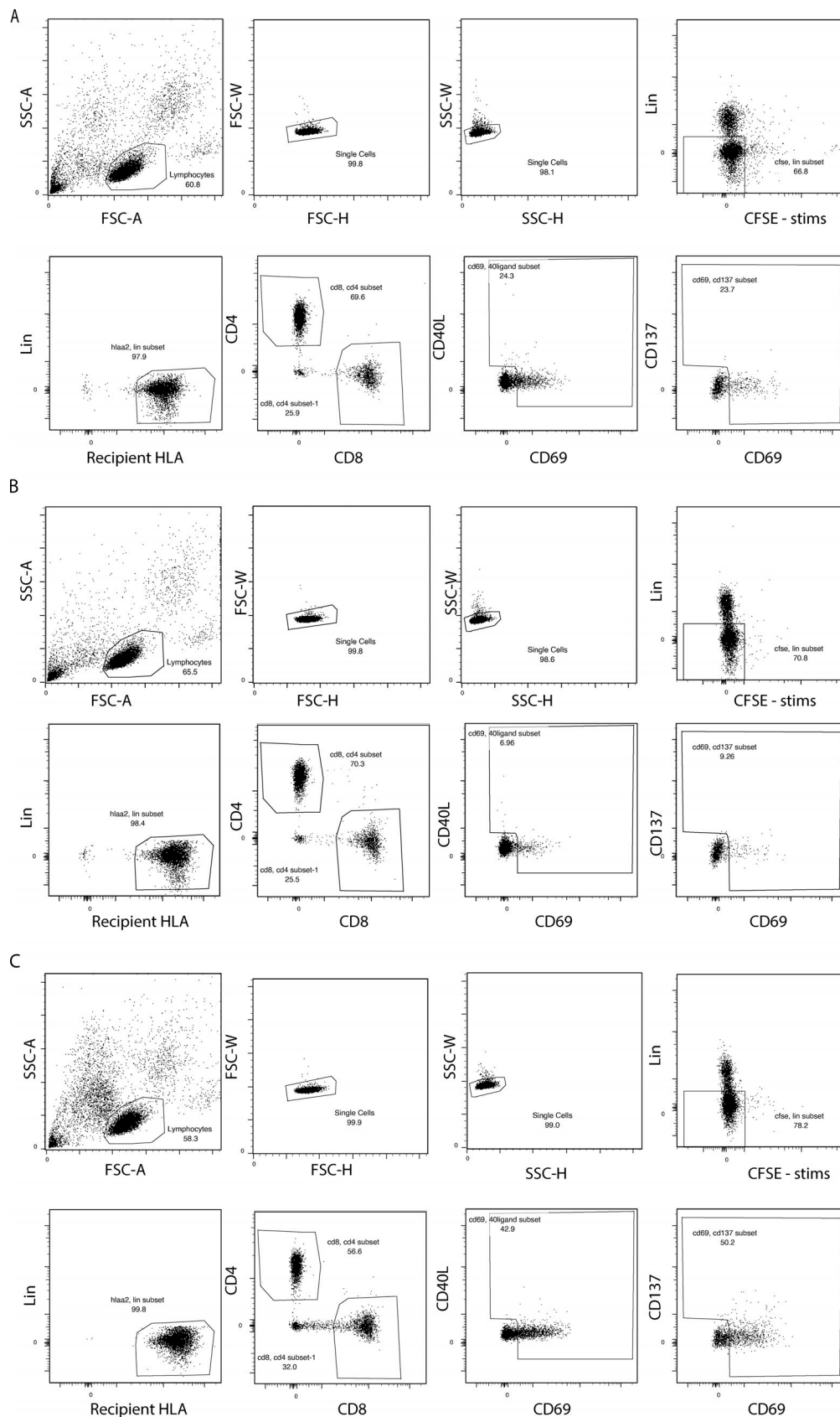


Figure S5. **Sorting strategy for bulk TCR sequencing.** (A–C) Representative sorting gates for bulk TCR sequencing of PBMCs from study participant P8 after stimulating with irradiated donor PBMCs in the absence of ACR (A), unstimulated in the absence of ACR (B), and unstimulated in the setting of ACR (C). FSC, forward scatter; SSC, side scatter.

Provided online are four tables. Table S1 shows the TCR specificity analysis with GLIPH. Table S2 shows the study participant HLAs. Table S3 lists the antibodies used for experiments. Table S4 lists the single-cell RNA/TCR quality assurance quality control.